Control of meiotic crossover interference by a proteolytic chaperone network

Authors:

Heejin Kim[1]*, Jaeil Kim[1]*, Namil Son[1], Pallas Kuo[2,6], Chris Morgan[3], Aurélie Chambon[4], Dohwan Byun[1], Jihye Park[1], Youngkyung Lee[1], Yeong Mi Park[1], John A. Fozard[3], Julie Guérin[4], Aurélie Hurel[4], Christophe Lambing[2,6], Martin Howard[3], Ildoo Hwang[1], Raphael Mercier[5], Mathilde Grelon[4], Ian R. Henderson[2], and Kyuha Choi[1†]

Affiliations:

[1]Department of Life Sciences, Pohang University of Science and Technology, Pohang, Gyeongbuk, Republic of Korea

[2]Department of Plant Sciences, University of Cambridge, Cambridge, CB2 3EA, UK

[3]John Innes Centre, Norwich Research Park, Norwich, UK

[4]Université Paris-Saclay, INRAE, AgroParisTech, Institut Jean-Pierre Bourgin (IJPB), 78000, Versailles, France

[5]Department of Chromosome Biology, Max Planck Institute for Plant Breeding Research, 50829 Cologne, Germany

[6]Rothamsted Research, Harpenden, UK

*These authors contributed equally to this work.

[†]**Correspondence:** kyuha@postech.ac.kr

Abstract

Meiosis is a specialized eukaryotic division that produces genetically diverse gametes for sexual reproduction. During meiosis, homologous chromosomes pair and undergo reciprocal exchanges, called crossovers, which recombine genetic variation. Meiotic crossovers are stringently controlled with at least one obligate exchange forming per chromosome pair, while closely-spaced crossovers are inhibited by interference. In *Arabidopsis*, crossover positions can be explained by a diffusion-mediated coarsening model, in which large, approximately evenly-spaced foci of the pro-crossover E3 ligase HEI10 grow at the expense of smaller, closely-spaced clusters. However, the mechanisms that control HEI10 dynamics during meiosis remain unclear. Here, through a forward genetic screen in *Arabidopsis* we identified *high crossover rate3* (*hcr3*), a dominant-negative mutant that reduces crossover interference and increases crossovers genome-wide. *HCR3* encodes J3, a co-chaperone related to HSP40, which acts to target protein aggregates and biomolecular condensates to the disassembly chaperone HSP70, thereby promoting proteasomal degradation. Consistently, we show that a network of HCR3 and HSP70 chaperones facilitates proteolysis of the key pro-crossover E3 ligase HEI10, thereby regulating interference and the recombination landscape. These results reveal a new role for the HSP40/J3-HSP70 chaperones in regulating chromosome-wide dynamics of recombination via control of HEI10 proteolysis.

Main Text

Meiotic recombination is initiated by the formation of programmed DNA double-strand breaks (DSBs) that are repaired using homologous chromosomes as templates to generate crossovers or non-crossovers[1,2]. Despite the formation of excess DSBs, only a subset mature into crossovers via DNA repair, resulting in one obligate crossover per chromosome pair and wide spacing between crossovers in most eukaryotes[3]. Two pathways, class I and class II, mediate crossover formation and positioning[3]. The class I pathway facilitates most crossovers and depends on the conserved pro-crossover ZMM proteins (named after *Saccharomyces cerevisiae* Zip1–4, Mer3, and Msh4–5) and the MutL protein homolog 1 (MLH1)–MLH3 heterodimeric endonuclease (MutLγ)[2,3]. ZMM proteins stabilize recombination intermediates such as displacement loops and double Holliday junctions, and recruit MutLγ to resolve crossovers[4]. Class I crossovers are subject to interference that spaces adjacent events wider than expected at random[5]. In contrast, class II crossovers are non-interfering and depend on the endonuclease MUS81[6]. Non-interfering crossovers are limited by multiple anti-recombination factors, including the FANCM and RECQ4A/4B helicases in plants[7,8].

Among ZMMs, the ZIP3/HEI10 (Human Enhancer of Invasion-10) family of meiotic SUMO and/or ubiquitin E3 ligases plays a key role in controlling interference-sensitive crossover number and position in a dosage-dependent manner[9–17]. HEI10 is initially loaded on early-leptotene chromosomes and becomes gradually enriched on the synaptonemal complex (SC), a proteinaceous structure that assembles between homologous chromosomes[16,18]. In *Arabidopsis* (*Arabidopsis thaliana*), HEI10 E3 ligases are proposed to diffuse along the SC and co-localize with hundreds of recombination intermediates as small foci at synapsed early-pachytene[18]. Like biomolecular condensates[19], HEI10 proteins eventually concentrate to late-pachytene designated crossover sites as one or a few large foci, at the expense of smaller foci[16,18]. A diffusion-mediated HEI10 coarsening model has been proposed to explain these dynamics, control of crossover number and interference[18]. In *Arabidopsis*, genetic disruption of SC transverse filament proteins abolishes interference and increases class I crossovers[20,21]. HORMA domain proteins of SC axis elements

are required to promote class I crossovers and mediate interference[22,23]. Interfering crossovers are limited by HCR1 (HIGH CROSSOVER RATE1, also named PROTEIN PHOSPHATASE X 1 [PPX1]) that potentially dephosphorylates HEI10 in *Arabidopsis*[24]. Consistently, post-translational modifications of pro-crossover factors, such as phosphorylation, SUMOylation, ubiquitination, and proteasomal proteolysis, have been implicated in controlling meiotic recombination in *Saccharomyces cerevisiae*, *Schizosaccharomyces pombe*, *Caenorhabditis elegans* and mouse[17,25–32]. However, the molecular mechanisms that mediate the proteolysis and dynamics of HEI10, the key pro-crossover factor during crossover control in plants, are largely unknown.

Genetic identification of *hcr3*

To identify new regulators of crossover patterning, we performed a high-throughput forward genetic screen for *high crossover rate* (*hcr*) mutants using a fluorescent seed recombination reporter line (*420*) and ethylmethane sulfonate-mediated mutagenesis in *Arabidopsis* (**Fig. 1a** and **Extended Data Fig. 1**)[24]. *hcr3* and *hcr3* heterozygous (*hcr3/+*) plants showed higher *420* crossover frequency than wild-type Columbia-0 (Col), indicating a dosage effect of *hcr3* (*t*-test, all $P<8.76\times10^{-6}$) (**Fig. 1b** and **Supplementary Table 1**). Using bulk sequencing of *hcr3* BC_1F_2 segregants, we determined that *hcr3* harbors a missense mutation (G-to-A) in *J3* (At3g44110) (**Fig. 1c** and **Extended Data Fig. 1d**). *J3* encodes a class A HSP40 (HEAT SHOCK PROTEIN 40) co-chaperone with an N-terminal J domain (J) followed by a glycine and phenylalanine-rich region (G/F), four copies of a CxxCxGxG zinc finger motif (ZnF), and a C-terminal peptide-binding fragment (C) (**Fig. 1c**)[33]. The *hcr3* mutation caused an amino acid substitution from glycine to arginine (G155R) in the first conserved ZnF (**Fig. 1c** and **Extended Data Figs. 2**–**3**). Class A HSP40 proteins form dimers through dimerization domains in their C termini (**Fig. 1c** and **Extended Data Fig. 3**)[34]. HSP40 protein dimers provide substrate specificity for the HSP70 chaperone machinery and cooperate with nucleotide exchange factor, HSP90, or HSP100/ClpB family members, to mediate proteome quality control pathways, including protein disaggregation and degradation[33–36].

hcr3 is a dominant-negative allele of *J3*

To further investigate the role of J3 in meiotic recombination, we obtained two *j3* T-DNA insertion mutants, *j3-1* and *j3-3*, which are loss-of-function alleles with no functional transcripts detected in RNA sequencing (RNA-seq) and RT-PCR analyses (**Fig. 1c** and **Extended Data Fig. 4a**–**e**). Both mutants were recessive and late-flowering, as previously observed [37], and showed increased crossover frequencies in *420* and six additional fluorescence-tagged line intervals (FTLs)/CTLs (Col Traffic Lines), compared to wild type (*t*-test, all $P<1.88\times10^{-3}$) (**Fig. 1d**, **Extended Data Figs. 4i,j, 5a,b** and **Supplementary Tables 2**–**5**). Complementation using a *J3* genomic fragment (*J3::Myc-J3*) reduced *420* crossover frequency of *j3-1* (25 cM) to the wild-type level (20 cM) (*t*-test, all $P>0.1$) (**Fig. 1d** and **Supplementary Table 2**). In addition, we observed that both *j3-1* and *j3-3* T-DNA alleles exhibited reduced pollen grains per anther (~63%), reduced number of seeds per silique (~ 81%), and approximately 30% chromosomal abnormalities in male meioctyes, including chromosome fragmentation at anaphase I (**Extended Data Fig. 6**), suggesting that J3 is required for flowering control, male gametogenesis, meiotic chromosome segregation, and seed development. *hcr3* plants shared the late flowering phenotype with *j3* knockout alleles (*t*-test, all $P<5.05\times10^{-9}$), but showed normal meiotic chromosome segregation, pollen, and seed development (**Extended Data Figs. 4i,j** and **6**). Interestingly, the *hcr3* point mutant allele showed higher *420* crossover frequency (30 cM) than the *j3* T-DNA knockout alleles (25 cM) (**Fig. 1b,d** and **Extended Data Fig. 5e**), indicating that *hcr3* is a dominant-negative allele of *J3*. Consistently, primary transgenic (T_1) plants expressing the $J3^{G155R}$ allele under the *J3*, constitutive *RPS5A* (*RIBOSOMAL PROTEIN 5A*) or meiotic prophase I gene promoters in the Col background showed higher *420* and *CTL5.14* crossover frequencies than Col and T_1 plants expressing *J3* (*t*-test, all $P<2.09\times10^{-3}$) (**Fig. 1e,f** and **Supplementary Tables 6**–**7**). Using *SPO11-1::*$J3^{G155R}$ transgenic plants expressing $J3^{G155R}$ from the meiotic *SPO11-1* promoter, we found that $J3^{G155R}$ transcript levels correlate with *CTL5.14* crossover frequencies (R^2 0.84, P=0.03, r=0.91) (**Fig. 1g**), demonstrating a dosage effect of $J3^{G155R}$ expression in increasing crossover frequency.

$J3^{G155R}$ dominantly inhibits the role of J3 and J2 in limiting crossovers

Arabidopsis encodes a *J3* paralog, *J2* (At5g22060) (**Extended Data Figs. 2** and **4**). J3 and J2 proteins share 90% amino acid sequence identity, leading our anti-J3 antibody to recognize both J3 and J2 proteins in immunoblot analysis (**Extended Data Figs. 2b,c** and **4f**–**h**). RNA-seq analysis revealed that the transcript level of *J3* is approximately four-fold higher than that of *J2* in seedlings and flower buds (**Extended Data Fig. 4c,e**). Consistently, our immunoblot analysis using the anti-J3 antibody detected the remaining J2 proteins in *j3-1* and *j3-3* knockout mutants, compared to the sum of J3 and J2 proteins in the wild type (*t*-test, all $P < 1.36\times10^{-2}$) (**Extended Data Fig. 4g,h**). In contrast, we detected approximately 60–80% (in seedlings) to wild-type levels (in flower buds) of J3 proteins in *j2-2*, a T-DNA insertion mutant that does not produce functional *J2* transcripts, compared to the wild type (**Extended Data Fig. 4a**–**h**). We observed that *j2-2* exhibited normal crossover frequency, flowering time, pollen viability, and fertility, suggesting that the more abundantly expressed J3 proteins function redundantly with J2 and compensate for their absence in *j2-2* (**Extended Data Figs. 4i,j, 5c,d, 6** and **Supplementary Table 4,8**). Consistently, *j3-1 j2-2/+* (25 cM) and *j3/+ j2-2* (20 cM) plants showed the same *420* crossover frequency as *j3-1* (25 cM) (*t*-test, $P=0.78$) and *j2-2* (20 cM) (*t*-test, $P=0.58$) plants, respectively (**Extended Data Fig. 5d** and **Supplementary Table 8**), suggesting that the increased crossover frequency depends on *j3-1*. However, transgenic *J3::J2*^{G156R} plants expressing *J2*^{G156R} under the *J3* promoter, mimicked the dominant-negative *hcr3* allele, showing an increased *420* crossover frequency similar to *hcr3* (*t*-test, $P=4.23\times10^{-8}$), and transgenic T_1 plants expressing *J2* in the *j3-1* mutant under the *J3* promoter restored *420* crossover frequency to wild-type levels (*t*-test, $P=0.74$) (**Extended Data Fig. 5e** and **Supplementary Table 9**). Furthermore, we observed that meiotic knockdown of *J2* in the *j3-1* background using meiosis-specific miRNA-induced gene silencing (meiMIGS) resulted in higher *420* crossover frequency than that in *j3-1* (*t*-test, $P=1.14\times10^{-4}$) (**Extended Data Fig. 5e** and **Supplementary Table 9**), demonstrating functional redundancy between *J2* and *J3* for crossover formation, with J3 playing a major role. Consistent with these findings, we also observed that *j3-1 j2-2/+* and *j3-1/+ j2-2* plants exhibited more severe defects in pollen grain and seedling development compared to *j3-1* and *j2*-2 single mutants, with approximately 5% of the progeny showing seedling lethality (**Extended Data Fig. 6a**–**f**). These results suggests that the majority of

j3-1 j2-2 mutants result in pollen, embryo, and seedling lethality, as described previously[38]. In addition, our yeast two-hybrid and co-immunoprecipitation assays revealed that the dominant-negative $J3^{G155R}$ proteins form dimers with both wild-type J3 and J2 proteins (**Extended Data Fig. 5f**–**h**). Taken together, these results suggest that $J3^{G155R}$ proteins produced by the *hcr3* allele increase crossovers in a dosage-dependent manner by dimerizing with J3 and J2 proteins and dominantly inhibiting J3/J2-HSP70 chaperone network-mediated activity.

hcr3 increases crossover frequency along chromosomes in male and female meiosis

Next, we investigated the genome-wide effect of *hcr3* on crossover frequency using a set of recombination reporter CTLs/FTLs located in multiple genomic regions (**Fig. 2a**). Sixteen seed-CTLs and three pollen-FTLs on distal chromosome regions showed higher crossover frequencies in *hcr3* than wild type (Col) (*t*-test, all $P<2.18\times10^{-3}$), whereas three CTLs spanning centromeres showed unchanged or moderately reduced crossover frequency (*t*-test, *CTL2.21* $P=1.21\times10^{-3}$, *CTL4.1* $P=1.15\times10^{-3}$, *CTL5.5* $P=0.25$) (**Fig. 2b,c** and **Supplementary Tables 10**–**11**). This indicates that *hcr3* promotes crossovers within the chromosome arms, but to a lesser extent within the pericentromeric and centromeric regions. To investigate the effect of HCR3 on male and female meiotic crossover recombination, we performed reciprocal crosses between *420 GR/++* Col, *hcr3*, or *J3::J3*^{G155R} plants with Col. We observed that *hcr3* and *J3::J3*^{G155R} showed higher *420* crossover frequencies in both male and female meiosis compared to the wild type (*t*-test, all $P<4.24\times10^{-5}$) (**Fig. 2d** and **Supplementary Table 12**), demonstrating that HCR3 limits recombination in both male and female meiosis.

J3^{G155R} expression increases crossovers genome-wide

To further investigate the effect of *J3*^{G155R} */hcr3* allele on the genomic crossover landscape at high resolution, we performed genotyping-by-sequencing (GBS) of F_2 individuals from self-pollinated F_1 plants derived from a cross between a *J3::J3*^{G155R} Col transgenic line (T_1#4), and the polymorphic Landsberg *erecta* (L*er*) accession, as well as F_2 individuals from Col×L*er* F_1 plants, which serves as a wild type control (**Extended**

Data Fig. 7a,b and **Supplementary Table 13**)[24,39,40]. *J3*^{G155R} led to approximately twice as many crossovers across the genome and on each chromosome in *J3::J3*^{G155R} Col×L*er* F_2 individuals (T_1#4, n = 96) compared to Col×L*er* F_2 plants (n = 240) (t-test, all $P<9.43\times10^{-13}$) (**Fig. 3a,b, Extended Data Fig. 7c,d** and **Supplementary Table 14**). We also performed GBS of F_2 individuals of two independent *J3::J3*^{G155R} Col×L*er* plants (T_1#6, n = 48, T_1#8 n = 48) and one *SPO11-1::J3*^{G155R} Col×L*er* plant (T_1#1, n = 96), which revealed that three independent *J3*^{G155R} transgenes elevated crossovers genome-wide by approximately two-fold (t-test, all $P<2.19\times10^{-5}$) (**Extended Data Fig. 8** and **Supplementary Table 13**–**14**). The additional crossovers occurred along the chromosome arms but were still suppressed around centromeres (**Fig. 3b**, **Extended Data Figs. 7d** and **8d,e**), similar to the crossover frequency of CTLs analysed in *hcr3* (**Fig. 2b**–**d**). Sex-specific crossover maps from reciprocal crosses between *J3*^{G155R} Col×L*er* F_1 and L*er* revealed that *J3*^{G155R} increases crossover approximately two-fold in both male and female meiosis (t-test, all $P<1.30\times10^{-3}$) (**Fig. 3c,d, Extended Data Fig. 7e,f** and **Supplementary Table 15**), confirming that *J3*^{G155R} exerts the same effects on male and female crossovers.

We observed that *hcr3 fancm* and *hcr3 recq4a recq4b* mutants have higher *420* and *I3bc* FTL interval crossover frequencies, respectively, compared to *hcr3*, *fancm*, and *recq4a recq4b* (*recq4a/4b*) (t-test, all $P<3.12\times10^{-4}$) (**Fig. 4a,b** and **Supplementary Tables 17**–**18**). *J3*^{G155R} also resulted in additively increased crossovers in *recq4a/4b* Col×L*er* F_1 hybrid plants (t-test, all $P<3.63\times10^{-3}$) (**Fig. 3e,f, Extended Data Fig. 7g,h** and **Supplementary Table 16**), which is similar to the combined effects of *HEI10* overexpression and *recq4a recq4b* mutations on crossover number and distribution (**Fig. 3g,h**)[15]. These results imply that HCR3 acts in parallel to the RECQ4A/4B and FANCM anti-crossover pathways and may restrict the HEI10-dependent class I crossovers.

To compare the effects of *j3* knockout and the *J3*^{G155R} transgene on meiotic crossovers, we sought to map crossovers genome-wide in the *j3* knockout background using the GBS approach (**Extended Data Fig. 9**). To achieve this, we generated new *j3* null alleles of *j3-5*, *j3-6*, and *j3-7* with premature stop codons in L*er*

background using CRISPR/Cas9 mutagenesis (**Extended Data Fig. 9a**). Like *j3-1* and *j3-3* in the Col background, the *j3-5* to *j3-7* alleles in L*er* showed reduced pollen viability and seed number per silique (*t*-test, all $P<1.43\times10^{-5}$) (**Extended Data Fig. 9b**–**d**). We observed that *420* crossover frequency was increased in *j3-1* Col×*j3-5* L*er* F_1 hybrids, compared to wild type and *j3* heterozygous Col/L*er* hybrids (*t*-test, $P=1.19\times10^{-7}$) (**Extended Data Fig. 9e**). Our genome-wide crossover mapping analysis of *j3-1*×*j3-5* F_2 individuals ($n = 96$) revealed that *j3* knockout increased the number of crossovers by approximately 30% on each chromosome (*t*-test, all $P<1.98\times10^{-2}$), and across the genome (*t*-test, $P=2.08\times10^{-9}$) compared to Col×L*er* F_2 plants (n=240) (**Extended Data Fig. 9f**–**i**). This suggests that expression of the $J3^{G155R}$ transgene inhibits both J3 and J2 proteins, thereby increasing crossovers more than *j3* knockout alone.

***hcr3* increases class I crossovers and decrease interference**

To gain further genetic insight into the effect of *hcr3* on class I and class II crossovers, we generated the *hcr3 hei10, hcr3 zip4,* and *hcr3 mus81* double mutants (**Fig. 4a,c**). *hcr3 hei10* and *hcr3 zip4* showed the same suppressed *420* crossover frequencies as *hei10* and *zip4* single mutants, indicating that the increased crossovers in *hcr3* are dependent on HEI10 and ZIP4 (**Fig. 4a** and **Supplementary Table 17**). In contrast, *hcr3 mus81* showed an approximate 12.1% reduction in *I1bc* crossover frequency compared to *hcr3*, as *mus81* showed an approximate 15.5% reduction compared to wild type (**Fig. 4c** and **Supplementary Table 19**). These genetic results demonstrate that HCR3 predominantly restricts class I interfering crossovers.

To determine the effect of *hcr3* on interference, we measured the crossover interference ratio (IFR) using three-color pollen FTLs (*I1bc*, *I3bc*, and *I5ab*), which allow mapping genetic distance of a test interval with and without a crossover in the adjacent interval[24,41]. The interference ratios increased as the incidence of double crossovers increased in *hcr3*, compared to wild type (*t*-test, all $P<2.55\times10^{-3}$) (**Fig. 4d,e** and **Supplementary Table 11**), indicating that interference strength is decreased in *hcr3* but not completely abolished. Interfering crossovers in *Arabidopsis* are sensitive to changes in ambient temperature, showing a moderate increase at higher temperature (28°C), compared to an optimal growth temperature (18–

20°C)[42,43]. We observed that *hcr3* displayed higher crossover frequencies in *I3bc* and *I5ab* at both optimal and higher temperatures than wild type (**Fig. 4f** and **Supplementary Table 20**), again supporting that HCR3 inhibits formation of interfering crossovers.

hcr3 and *j3* increase the numbers of MLH1 foci per meiocyte

Because the additional crossovers in *hcr3* depend on HEI10 (**Fig. 4a**)[11,15], we performed transcriptomic (RNA-seq) analysis in Col, *hcr3*, *j3-3*, and *j2-2* flower buds smaller than 0.6 mm to examine whether *hcr3* and *j3* affect *HEI10* transcription. The transcript levels of *HEI10* were not altered in *hcr3*, *j3-3*, or *j2-2*, but were increased in *hcr2*, as observed previously[39] (**Fig. 4g**). To confirm the effects of *hcr3* and *j3* on *HEI10* transcription during meiosis, we purified male meiocytes and performed RT-qPCR analysis in Col, *hcr2*, *hcr3*, *j3-1*, *j3-3*, and *j2-2* plants. Again, we observed that *HEI10* transcript levels were not changed in *hcr3*, *j3-1*, *j3-3*, and *j2-2* compared to wild type (*t*-test, all $P>0.1$), but were increased in *hcr2* meiocytes (*t*-test, $P=4.34\times10^{-10}$) (**Fig. 4h**). Cytological analysis showed that meiotic axis formation, synapsis, chromosome segregation, and pollen viability are normal in *hcr3* mutants (**Extended Data Figs. 6a,b,f, 10a** and **Supplementary Table 21**). The DSB marker, RAD51, remained unchanged in *hcr3* male meiocytes (Wilcoxon test, $P=0.4$) (**Extended Data Fig. 10b,c** and **Supplementary Table 22**), but the number of MLH1 foci, a marker of class I crossover sites, increased in *hcr3* compared to wild type at late-pachytene, diplotene, and diakinesis (Wilcoxon test, all $P<1.23\times10^{-4}$) (**Fig. 5a,b** and **Supplementary Table 23**). Similar to *hcr3*, we also observed an increase in the number of MLH1 foci per cell in *j3-1* and *j3-3* knockout mutants (Wilcoxon test, *j3-1* $P=1.15\times10^{-2}$, *j3-3* $P=5.88\times10^{-3}$) (**Extended Data Fig. 9j** and **Supplementary Table 23**), demonstrating that HCR3 limits class I crossovers.

HEI10 foci are increased and more closely spaced per bivalent in *hcr3*

Increased MLH1-immunostaining is consistent with *hcr3* increasing the abundance of HEI10, or other ZMM factors. Therefore, we quantified immunostained foci for HEI10 in *hcr3* using super-resolution structured illumination microscopy with co-immunostaining for ZYP1, a marker of the synaptonemal

complex (**Fig. 5c,d**)[18]. We observed an increase in the number of late-pachytene HEI10 foci per bivalent in *hcr3* (Wilcoxon test, $P<5.97\times10^{-7}$) (**Fig. 5c,d**). Moreover, the distance between adjacent HEI10 foci along chromosome axes decreased, with a high coincidence of closely-spaced HEI10 foci in *hcr3* (mean=16.7 μm), compared to the wild type (mean=23.0 μm, Wilcoxon test, $P<2.64\times10^{-7}$) (**Fig. 5d**). Because our recent HEI10 coarsening model can explain the effects of HEI10 expression levels on crossover number and interference[18], we tested whether the effect of *hcr3* on HEI10 foci is consistent with this model. We ran simulations using the same parameter values from[18] and *hcr3* simulations, which were identical to Col simulations but with 1.3× the initial amount of HEI10 along the SC and at recombination intermediate sites. *hcr3* simulation outputs displayed an increased number and closer spacing of crossovers compared to Col simulations (Wilcoxon test, all $P<2.20\times10^{-16}$) (**Fig. 5d**)[18]. However, we note that closely-spaced HEI10 foci were over-represented in *hcr3* experimental data compared to crossovers in *hcr3* simulations. This suggests that the effects of *hcr3* on crossovers are, at least in part, mediated by changes in HEI10 abundance and/or dynamics. Correspondingly, male- and female-specific crossover maps revealed that *J3::J3*^{G155R} Col×L*er* F_1 plants show more crossovers and shorter physical distances between crossovers on the same chromosomes (male mean=7.7 Mb, female mean=10.0 Mb) compared to Col×L*er* F_1 plants (male mean=11.4 Mb, female mean=13.3 Mb, Wilcoxon test, all $P<1.00\times10^{-2}$) (**Figs. 3c,d, 5e, Extended Data Fig. 7e,f** and **Supplementary Table 24**). Notably, as in wild-type Col×L*er* F_1 plants, the crossovers in *J3::J3*^{G155R} Col×L*er* F_1 plants were more widely spaced than expected from a random distribution (Wilcoxon test, *J3*^{G155R}, all $P<9.70\times10^{-6}$), indicating that *J3*^{G155R} reduces but does not eliminate crossover interference (**Fig. 5e** and **Supplementary Table 24**), consistent with *hcr3* decreasing interference in pollen tetrad analysis (**Fig. 4d,e**).

HCR3 localizes on the synaptonemal complex and physically interacts with HEI10

By co-immunostaining for J3, ASY1, ZYP1, and DNA during meiosis, we found that both J3 and J3^{G155R} signals localize to the nucleus, surrounding the axis (ASY1) and transverse elements (ZYP1) of the SC signals at leptotene, zygotene, and pachytene stages in Col and *hcr3*, with weak signals for the remaining

J2 proteins in *j3-1* (**Fig. 6a** and **Extended Data Fig. 10d**). These results prompted us to investigate whether the J3 co-chaperone interacts with meiotic recombination proteins using yeast two-hybrid assays. Indeed, both J3 and J3^{G155R} interacted strongly with HEI10, PTD, MSH5, and ZIP4, and weakly with MER3, but not with SHOC1 or MLH1 (**Fig. 6b** and **Supplementary Table 25**). We also detected an interaction between J3 and J3^{G155R} with other meiotic proteins such as ASY1, an axis element of SC, indicating that J3 is a broad protein partner, as expected for class A HSP40 co-chaperones (**Supplementary Table 25**)[34]. We confirmed the protein interactions of J3 and J3^{G155R} with HEI10, PTD, and MSH5 *in planta* using co-immunoprecipitation and TurboID-based proximity labeling assays in *Arabidopsis* protoplasts (**Extended Data Fig. 11**).

To investigate the interactions of J3 and J3^{G155R} with HEI10 at recombination intermediates *in vivo*, we performed co-immunostaining of J3, J3^{G155R}, and HEI10, along with ZYP1, during pachytene in wild-type and *hcr3* male meiocytes using anti-J3, anti-HEI10, and anti-ZYP1 antibodies (**Fig. 6c**). We observed that the majority of immunostained signals of small and large HEI10 foci at recombination intermediates co-localized with the signals of J3/J2 in wild type and J3^{G155R}/J2 in *hcr3* at the mid-pachytene stage (**Fig. 6c**). Furthermore, our co-immunofluorescence analysis of pollen mother cells using epitope-tagged HA and Myc antibodies confirmed the co-localization of distinct HEI10-Myc foci with HA-J3 and HA-J3^{G155R} at late-pachytene stages in *HEI10::HEI10-Myc*, *HEI10::HEI10-Myc hcr3*, *J3::HA-J3 HEI10::HEI10-Myc*, and *J3:HA-J3^{G155R} HEI10::HEI10-Myc* plants (**Extended Data Fig. 12a,c**). We also observed that immunostained J3 signals co-localize with HEI10-Myc foci at diplotene and diakinesis in *HEI10::HEI10-Myc* plants (**Extended Data Fig. 12b**). The co-localization of J3 and HEI10 foci at mid to late-pachytene, diplotene, and diakinesis stages suggest that J3 may interact with dynamic HEI10 foci at recombination intermediate sites, developing crossover sites, and designated crossover sites.

HCR3 promotes degradation of HEI10 and pro-crossover factors

Because a J3 homolog, Ydj1, is required for protein degradation in budding yeast[35,44], we examined the effects of the *hcr3* and *j3-1* on protein turnover of HCR3-interacting ZMM proteins. We determined that HEI10, PTD, and MSH5 were more abundant in *hcr3* and *j3-1* than in the wild type when their encoding constructs were transiently expressed in protoplasts (*t*-test, all $P<1.89\times10^{-2}$) (**Fig. 7a,b**). Consistently, we detected higher protein levels of HEI10-Myc, PTD-Myc, and MSH5-Myc in transgenic plants co-expressing *HA-J3*^{G155R}, compared to transgenic plants co-expressing *HA-J3* (*t*-test, HEI10-Myc $P=4.47\times10^{-2}$, PTD-Myc $P=1.17\times10^{-2}$, MHS5-Myc $P=2.08\times10^{-3}$) (**Fig. 7c,d**). To investigate more direct effects of J3 and J3^{G155R} on HEI10 abundance, we transiently co-expressed Myc-J3 or Myc-J3^{G155R} with HEI10-HA in *j3-1* protoplasts, and then quantified HEI10 abundance by immunoblot analysis (**Fig. 7e,f**). We observed that transiently expressed Myc-J3 proteins led to decreased HEI10-HA levels in *j3-1* protoplasts, compared to empty vector transfections (*t*-test, $P=9.74\times10^{-3}$), and Myc-J3^{G155R} proteins maintained HEI10-HA levels in *j3-1* (*t*-test, $P=3.02\times10^{-3}$) (**Fig. 7e,f**), indicating that J3 facilitates HEI10 degradation. More importantly, immunoblot analysis using an anti-HEI10 antibody showed that endogenous HEI10 protein abundance is higher in *j3-1*, *hcr3*, and *J3::J3*^{G155R} transgenic plants than in wild type (*t*-test, all $P<4.70\times10^{-2}$) (**Fig. 7g,h**). These results suggest that HCR3 facilitates proteolysis of HEI10, PTD, and MSH5 and that the additional crossovers in *j3-1*, *hcr3*, and *J3::J3*^{G155R} plants are dependent on increased HEI10 abundance. Moreover, the effects of *hcr3* on crossover number and, to a lesser extent, on crossover interference through the increased HEI10 abundance are consistent with the HEI10-mediated coarsening model (**Fig. 5c,d**)[18].

HCR3 facilitates proteolysis of HEI10 through a HSP70 chaperone network

HSP40/J-protein dimers deliver specific substrates to HSP70 and interact with HSP70 through their J-domain, synergistically promoting HSP70 ATPase activity[33]. In agreement, we detected physical interaction of HCR3 and J3^{G155R} with *Arabidopsis* HSP70 *in vitro* and found that HCR3-HSP70 chaperones co-localize with HEI10, PTD, and MSH5 in the nucleus of protoplasts co-transfected with their encoding constructs (**Extended Data Fig. 13a,b,d**). We also found that J2, the J3 paralog, interacts with HSP70 and

HEI10 in co-immunoprecipitation and co-localization analyses (**Extended Data Fig. 13c,d**), further supporting the redundant role of J3 and J2 in restricting crossovers. Therefore, we investigated the role of *Arabidopsis* HSP70 in crossover formation by meiotic knockdown of *HSP70* genes (*HSP70-1* and *HSP70-3*) using meiMIGS (**Extended Data Fig. 13d**–**k**)[24,39,45]. We observed higher crossover frequencies in the *420*, *CTL1.17*, *CTL1.22*, *CTL3.15*, and *CTL4.7* FTL reporters (*t*-test, all $P<6.91\times10^{-6}$), and higher HEI10 abundance in *meiMIGS-HSP70* transgenic plants than in the wild type (*t*-test, $P=1.23\times10^{-2}$), concomitantly with lower transcript levels of nuclear *HSP70* genes (*t*-test, all $P<3.52\times10^{-2}$) (**Fig. 7i,j, Extended Data Fig. 13e**–**i** and **Supplementary Table 26**). In addition, we mapped crossovers genome-wide using GBS of *meiMIGS-HSP70* Col/L*er* F_2 individuals (T_1#1, n = 96) (**Extended Data Fig. 13j,k)**, which revealed that *meiMIGS-HSP70* resulted in an increase in the number of crossovers (8.92/F_2) across the genome compared to controls (*t*-test, $P=8.43\times10^{-5}$) (**Extended Data Fig. 13j,k**), suggesting that HSP70 and J3/J2 cooperate to restrict crossovers.

Because HSP40-HSP70 chaperones target protein complexes, aggregates or biomolecular condensates to other co-chaperones, such as hexameric HSP100 disassembly machines (*Arabidopsis* HSP101) and HSP90, for degradation by cooperating with the ubiquitin-proteasome system[33,46], we examined the effect of the *hsp101* mutation on HEI10 abundance using immunoblot analysis. We observed that *hsp101* did not increase HEI10 abundance (*t*-test, $P=0.75$), crossover frequency (*t*-test, all $P>0.22$), or MLH1 foci (Wilcoxon test, $P=0.93$), compared to wild-type controls (**Extended Data Fig. 14**), suggesting that the HCR3-HSP70 chaperone network may facilitate HEI10 degradation and limit crossovers, potentially by cooperating with other co-chaperone machines such as HSP90 in *Arabidopsis*.

HCR3 mediates ubiquitin and SUMO modifications of HEI10 for degradation

To investigate how HCR3 mediates the protein turnover of HEI10, we examined the effect of *hcr3* on ubiquitin (Ub) and SUMO modifications of HEI10 using *HEI10::HEI10-Myc* and *hcr3 HEI10::HEI10-Myc* plants (**Fig. 7k,l**). Immunoprecipitation of HEI10-Myc and subsequent immunoblot analysis using Ub

and SUMO antibodies revealed that *Arabidopsis* HEI10 is modified by both ubiquitination and SUMOylation (**Fig. 7k,l**). Using an anti-Ub antibody specific for lysine 48 residue-linked Ub chains (K48-Ub) that triggers poly-ubiquitination-dependent proteasomal degradation, we observed lower levels of poly-Ub-conjugated HEI10-Myc proteins in *hcr3* than in the wild type, when the intensities of poly-ubiquitylated HEI10-Myc proteins were normalized by those of immunoprecipitated and unmodified HEI10-Myc proteins (*t*-test, $P=2.85\times10^{-3}$) (**Fig. 7k,l**). This result suggests that HCR3 promotes proteasomal degradation of HEI10 by facilitating its poly-ubiquitination. To further investigate ubiquitin-proteasome-dependent HEI10 degradation, we used the *Arabidopsis* protoplast transient expression system (**Extended Data Fig. 15**). In this system we transiently expressed either FLAG-tagged Ub (FLAG-Ub) or HEI10-HA, or both, for immunoprecipitation and immunoblot analysis of HEI10-HA. We detected shifted bands indicative of FLAG-Ub-conjugated HEI10-HA proteins when FLAG-Ub and HEI10-HA were co-expressed, which were not evident in controls (**Extended Data Fig. 15a**), suggesting that ubiquitin modification of HEI10-HA may be mediated by a ubiquitin E3 ligase and/or HEI10-HA itself. HEI10-HA proteins underwent rapid degradation in protoplasts since translation elongation was blocked by the treatment with cycloheximide. However, HEI10-HA degradation was delayed, and FLAG-Ub-conjugated HEI10-HA forms were increased upon treatment with the proteasome inhibitor MG132 (*t*-test, all $P<4.48\times10^{-2}$) (**Extended Data Fig. 15a**–**c**), indicating that HEI10 degradation depends on ubiquitin-proteasome system. Using an anti-SUMO1 antibody that recognizes SUMOylation in *Arabidopsis*, we also observed that poly-SUMOylated HEI10-Myc levels were decreased in *hcr3*, compared to the wild type (*t*-test, $P=3.05\times10^{-2}$) (**Fig. 7k,l**), suggesting that poly-SUMOylation may also mediate HEI10 degradation. Taken together, we propose that HCR3 facilitates poly-Ub and poly-SUMO modifications of HEI10 that promote its degradation.

Discussion

Formation of protein aggregates or biomolecular condensates is counteracted by HSP40-HSP70 disaggregation chaperones and proteasomes for dispersal and degradation[19,33,36,46,47]. Our findings suggest that the disaggregating machinery facilitates proteolysis of HEI10 and HCR3-interacting ZMMs at

recombination intermediate foci and SC to limit interfering crossover formation during *Arabidopsis* meiosis (**Fig. 7m**). The HEI10/ZIP3 E3 ligase family is involved in the SUMO-ubiquitin-proteasome relay for crossover control in mouse and budding yeast[25,31]. Mammalian genomes encode both a SUMO E3 ligase (RNF212) and a ubiquitin E3 ligase (HEI10) that function to control crossovers[12,13]. The RNF212-HEI10 pathway stabilizes a minority of crossover-designated recombination intermediates through RNF212 and destabilizes the majority of recombination intermediates through HEI10 for non-crossovers[12,13,31]. However, plants and the fungus *Sordaria* encode only the HEI10 family, while budding yeast and worms have only the ZIP3 family[4,9,10,14,16], suggesting a temporal or SUMO/ubiquitin switch activity of each family for selective stability and disruption of recombination intermediates. Our observations of ubiquitylated and SUMOylated HEI10 in the wild type and *hcr3* suggest that the HCR3-HSP70 chaperone network promotes HEI10 turnover and dynamics at recombination intermediate sites and along the SC by facilitating both poly-ubiquitination and poly-SUMOylation of HEI10 via HEI10 autoregulation and/or other E3 ligases. As HEI10 dosage and diffusion-mediated coarsening determine crossover number and interference in *Arabidopsis*[11,18], we propose that HCR3 co-chaperone molecules monitor the molecular status of HEI10 and growing HEI10-containing recombination foci along paired chromosomes for their disaggregation and degradation. We found that by increasing general HEI10 abundance within our mathematical coarsening simulations, along the SC and at recombination intermediate sites (akin to HEI10 overexpressor simulations), we were able to recapitulate experimental increases in HEI10 focus number in *hcr3* mutants, supporting a coarsening driven explanation for meiotic crossover patterning. Increased HEI10 abundance leads to a greater number of crossovers within the model by enabling a greater number of large HEI10 foci to stably persist until the end of prophase I. In an *hcr3* mutant, increased HEI10 abundance at recombination intermediate sites and along the SC would result from a lack of HCR3-mediated HEI10 proteolysis. HCR3-mediated proteolysis is presumably required to stringently maintain specific HEI10 protein levels and, thus, preserve wild-type levels of meiotic crossovers. This is supported by our immunoblot and cytological analyses of HEI10 abundance and positioning in *hcr3*. We also observed an increase in closely spaced HEI10 foci within our *hcr3* model, consistent with reduced CO interference, although we also note that

closely spaced HEI10 foci were overrepresented in our experimental data compared with our model, suggesting that *hcr3* may also play a role in modulating other coarsening parameters. For example, it is possible that HCR3-HSP70 chaperone activities, such as substrate unfolding and folding, contribute to the disassembly or recycling dynamics of HEI10 at foci, which allow diffusible HEI10 molecules to be remobilised between SC associated recombination foci. It will also be intriguing to explore using live imaging approaches[48] if and how HEI10 foci are degraded and/or dismantled at the majority of recombination intermediates via the HCR3-HSP70 chaperone network, with only a subset further stabilized at designated crossover sites.

Our findings on HCR3 provide more evidence that HEI10 is a major target of anti-crossover factors, such as HCR1 and HCR2 in the class I pathway[24,39]. We determined that the *hcr1 hcr3* double mutant has higher HEI10 abundance and crossover frequency than each of the single mutants (**Extended Data Fig. 16a,b** and **Supplementary Table 27**), consistent with HEI10 being post-translationally regulated in parallel by HCR1-catalyzed dephosphorylation and chaperone-mediated proteolysis. It is likely that during HEI10 coarsening[18,49,50], HCR1 phosphatase and its counteracting kinases determine phosphorylation status of HEI10[24]. Simultaneously, HCR3 may monitor the phosphorylation and conformational states of HEI10, and facilitates HEI10 modification through ubiquitination and SUMOylation to promote degradation. Hence, we propose that the tight regulation of HEI10 abundance is required to mediate crossover interference and inhibit close-spacing of crossovers that are sensitive to changes in temperature and genome ploidy[42,43,51]. Besides the disaggregating and proteolytic roles of heat-induced molecular chaperones comprising HSP40 and HSP70 in thermotolerance[33,36,46,47], our findings provide genetic and mechanistic insights into how the disaggregation chaperone network of J3/J2-HSP70 limits meiotic crossovers and regulates interference by promoting degradation of pro-recombination factors.

Methods

Plant materials

The *Arabidopsis* (*Arabidopsis thaliana*) Columbia-0 (Col) accession was used as the wild type. Plants were grown in controlled growth rooms (20°C, 50%–60% humidity, and 16-h-light/8-h-dark photoperiod). Fluorescence-tagged lines for scoring seed and pollen tetrads were used as described[52,53]. The T-DNA insertion lines *j3-1* (SALK_132923)[37], *j3-3* (SAIL_1292_G03.V1), *j2-2* (SALK_071563)[38], *zip4-2* (SALK_068052)[16], *mus81-2* (SALK_107515)[6], *hsp101* (SALK_066374)[54], and *hei10-2* (SALK_012624)[16] were provided by the Arabidopsis Biological Resource Center (ABRC). The *fancm-1*[7], *hcr1*, and *hcr2* mutants were used as described previously[24,39]. The mutants of *recq4a recq4b* in Col and L*er* accessions were used as described by Fernandes et al.[55]. Genotyping of *hcr3* was performed by PCR using oligonucleotides *hcr3*-geno F and R (**Supplementary Table 28**), followed by *Bam*HI (NEB, UK) restriction endonuclease digestion.

Genetic screening and mapping of *hcr3*

Genetic screening and mapping of ethyl-methyl sulfonate (EMS)-derived *hcr3* using the *420* (*GR/++*) fluorescent seed reporter were performed as described by Nageswaran et al.[24]. Approximately 10,000 seeds of *420 GR/++* hemizygote seeds were treated with 0.3% (v/v) EMS and incubated for 12 h at room temperature (20°C). Approximately 7,000 M_1 plants were grown and seeds of 12 M_1 plants were harvested and pooled for 600 M_2 pools. Approximately 150 seeds of each M_2 pool were pre-selected as *420/++* hemizygotes, grown, self-fertilized and used for *420* crossover frequency. To map the causal mutation of *hcr3*, the *hcr3* with the *420* reporter (*hcr3 GR/GR*) was crossed to Col plant. The back-crossed F_1 plants (*hcr3/+*; *420 GR/++*) were self-fertilized to produce BC_1F_2 populations (**Extended Data Fig. 1**). BC_1F_2 seeds were pre-selected as measurable *420/++* BC_1F_2 hemizygous plants under an epi-fluorescence microscope and grown. F_3 seeds from individual BC_1F_2 plants were harvested and used to measure the *420* crossover frequency (cM) using CellProfiler, equipped with an automatic seed scoring pipeline. Fifty BC_1F_2 plants with high crossover rates, like *hcr3* were selected and approximately 5 mg of BC_1F_3 seeds from each

BC_1F_2 individual were pooled and grown on 1/2 MS agar plates. Nuclear genomic DNA (gDNA) of pooled *hcr3* BC_1F_3 7-day seedlings was isolated and used for the preparation of a DNA sequencing library as described by Nageswaran et al.[24]. The SHOREmap (v.3.0) pipeline was used to map candidate mutations responsible for the *hcr3* phenotype, as described by Nageswaran et al.[24,56].

Plasmid construction for transgenic plants and transient assay

Plasmid construction in this study was performed using the Golden Gate cloning system as described by Nageswaran et al.[24] (**Supplementary Table 28**). For the complementation analysis of *j3*, the genomic regions of the *J3* promoter-5′-UTR, protein coding region, and 3′-UTR-terminator region were separately PCR-amplified and each PCR product was cloned to the universal Level 0 (Lv0) vector (pAGM9121). For N terminal Myc or HA tagging, Lv0 vector of the J3 protein coding region was assembled to Lv1 vector with Myc or HA vector, Lv0 vectors of the promoter-5′-UTR and 3′-UTR-terminator region. The Lv1 of *J3(J3promoter)::Myc-J3* was assembled to an Lv2 binary vector (pAGM4723) with the antibiotic resistant gene *BAR* containing an Lv1 vector (pICSL11017) and linker (pICH41744). The Lv2 vectors were electroporated into *Agrobacterium* strain GV3101-pSOUP and transformed into *Arabidopsis* by floral dipping.

To generate transgenic plants that express *J3* or $J3^{G155R}$ under the *J3* or meiotic gene promoters, the genomic sequences of different gene promoters, *J3* and $J3^{G155R}$ were cloned into the pAGM9121 vector using Golden Gate cloning. The Lv0 vectors for *J3* and meiotic gene promoters, *J3* or $J3^{G155R}$, were assembled into the Lv1 position 2 vector pICH47742 with the pICH41421. Each Lv1 vector was assembled into the pAGM4723 binary vector with pICSL11017 and pICH41744.

For *meiMIGS-HSP70* and *meiMIGS-J2* plants, cDNA regions of *HSP70-1*, *HSP70-3*, and *J2* were cloned into the Lv0 vector (pAGM9121) following amplification using forward primers that included the miR173 target sequence and reverse primers (**Supplementary Table 28**). The *DMC1* promoter and *MIGS-HSP70*

Lv0 vectors or the *SPO11-1* promoter and *MIGS-J2* Lv0 vectors were assembled into the Lv1 position 2 vector (pICH47742) with the *NOPALINE SYNTHASE GENE* (*NOS*) terminator (pICH41421). The Lv1 vector was assembled to the pAGM4723 binary vector with pICSL11017 and pICH41744.

To generate *j3* knockout alleles using CRISPR/Cas9 mutagenesis, Gateway *pEn-C1.1* (Addgene plasmid #61479) and *pDe-CAS9* (Addgene plasmid #61433) plasmids were used and two sgRNAs were cloned using complementary sgRNA oligonucleotides (**Supplementary Table 28**), as previously described[57].

For the *Arabidopsis* transient assay, the full-length protein coding region lacking stop codons of meiotic genes was cloned to pAGM9121 universal vector. The Lv0 vectors were assembled in the Lv1 vector (pICH4772), with the *35S* promoter (pICH51266), C-terminal epitope-tagged vector (pICSLl50010 or pICSL50009), and *NOS* terminator (pICH41421). For TurboID-based proximity labeling assays of TurboID-J3[58], TurboID clone was assembled to the N-terminal of *J3* in the Lv1 vector with Lv0 vectors of the *35S* promoters (protoplasts) or *J3* promoters (plants), *J3* coding region, and *NOS* terminator.

High-throughput measurement crossover frequency and interference ratio

In the seed FTL system, crossover frequency was measured using a CellProfiler image analysis pipeline that allows for the analysis of fluorescent and non-fluorescent seeds from *FTL/++* hemizygote plants. CellProfiler detects and analyzes the numbers of green-only fluorescent seeds (N_{Green}), red-only fluorescent seeds (N_{Red}), and total seeds (N_{Total})[59]. Crossover frequency (cM) is calculated using the formula: $cM = 100 \times (1 - [1 - 2(N_{Green} + N_{Red})/N_{Total}]^{1/2})$[53,60]. In the pollen tetrad FTL system, DeepTetrad, a deep learning-based image analysis pipeline was used for the measurement of crossover frequency and interference ratio (IFR) in two- or three-color FTLs, as described by Berchowitz and Copenhaver[41] and Lim et al.[41,61]. Using three-color FTLs that have two intervals IFR was calculated as the ratio of the map distance with adjacent crossover to the map distance without adjacent crossover. One sided Welch's *t*-test was used to test whether crossover frequency and IFR varied significantly among genotypes.

Genotyping-by-sequencing (GBS) for mapping genomic crossover sites

For sex-average crossover maps, Col and *J3::J3*^{G155R} Col in *420* background were crossed with L*er* to produce Col×L*er* and *J3::J3*^{G155R}/+ Col×L*er* F_1 hybrid plants, respectively. F_1 plants were allowed to self-fertilize for the production of F_2 individuals. For sex-specific crossover maps, the Col×L*er* and *J3*^{G155R}/+ Col×Ler F_1 hybrid plants were reciprocally crossed with L*er*. The backcrossed F_1 individuals were used for GBS. For crossover maps in the *recq4a recq4b* background, the *J3*^{G155R} Col plant was crossed with *recq4a recq4b* Col, and then the F_1 plant (*J3*^{G155R} /+ *recq4a*/+ *recq4b*/+) was crossed with the *recq4a recq4b* L*er* plant to produce *J3*^{G155R} /+ *recq4a recq4b* Col×Ler F_1 hybrid. Individual plants were grown on soil for 3 weeks. The gDNA was extracted from two to three adult leaves per individual plant using the CTAB method for the preparation of sequencing libraries as described by Nageswaran et al.[24] and Ziolkowski et al.[11]. Briefly, 150 ng gDNA from each F_2 plant was quantified using Qubit dsDNA Broad Range assay kit (ThermoFisher) and fragmented using dsDNA Shearase (Zymo Research) and used to generate one sequencing library per plant. The 96 barcoded libraries were pooled and subjected to paired-end 150-bp sequencing using an Illumina HiSeqX instrument (Macrogen, Korea). The TIGER pipeline was applied to analyze the sequencing data and map precisely crossovers as described by Rowan et al.[40].

RNA sequencing

RNA extraction and sequencing library construction were performed as described by Choi et al.[62]. Total RNA was extracted from the seedlings and unopened floral buds that were smaller than approximately 0.6 mm using RNeasy Plant mini kit (QIAGEN). A Ribo-Zero magnetic kit (MRZPL116, Epicentre) was used for rRNA depletion. In addition, 50 ng of rRNA-depleted RNA was used to construct sequencing libraries using a ScriptSeq v2 RNA-seq Library Preparation Kit (SSV21124, Epicentre). Twelve PCR cycles were used for amplification of the libraries using ScriptSeq Index PCR Primers (RSBC10948, Epicentre). Three replicates of the RNA-seq libraries were generated for each genotype with different indexes. Sequencing was conducted on an Illumina HiSeq instrument (BGI, Hong). Adapter sequences were trimmed from the

raw reads with Trim Galore (v. 0.6.6) with parameters -q 0 --stringency 3 --length 20. Trimmed reads were aligned to the TAIR10 reference using STAR (v. 2.7.3) with default parameters. The number of reads mapped to exons was calculated using featureCounts (v. 2.0.1) with default parameters[63]. Differentially expressed genes (DEGs) and sequencing reads were analyzed among meiosis-related genes (in-house list) with the R package *DESeq2* using a Benjamini–Hochberg adjusted *P*-value < 0.01 as cutoff[64].

RT-qPCR analysis

Male meiocytes were isolated from stage 9 floral buds by squeezing them between a glass slide and coverslip, as previously described[65]. Total RNA from purified male meiocytes or floral buds smaller than 0.6 mm was isolated using TRIzol reagent (Invitrogen) and used for RT-qPCR using a reverse transcription kit (Enzynomics, EZ405S). Quantitative PCR was performed using a CFX real-time PCR detection system (Bio-Rad). *TUB2 (TUBULIN BETA CHAIN2)* was used as a reference for normalization. RT-qPCR was conducted with two or three biological replicates and three technical repeats per replicate.

Purification of J3 protein and antibody generation

The full-length *J3* coding sequence (At3g44110) was amplified from *Arabidopsis* cDNA using pQE-J3_F and pQE-J3_R primers. The PCR product was then cloned into the pQE-80L expression vector using the *Bam*HI and *Hin*dIII restriction sites via the Gibson assembly cloning system to generate an N-terminal 6x-His tagged recombinant protein. The resulting construct was transformed into *Escherichia coli* strain BL21 (DE3) RIL and the recombinant J3 protein was purified as previously described[39]. A polyclonal antibody against the purified recombinant J3 protein was raised in mice (Abclon, Korea).

Immunocytological analysis

Chromosome spreads of pollen mother cells from fixed buds and staining with DAPI were performed as described by Chelysheva et al.[66]. Immunostaining of MLH1 was performed on acetic acid chromosome spreads using fixed buds as described by Chelysheva et al.[66]. Immunostainings of ASY1, RAD51, ZYP1,

J3 and HEI10 were performed using fresh floral buds as described by Lambing et al.[22] and by Morgan et al.[18] for late-pachytene nuclei. The following antibodies were used: α-ASY1 (rat, 1:500 dilution, guinea-pig, 1:500 dilution), α-ZYP1 (rabbit, 1:200 dilution, rat, 1:500 dilution), RAD51 (rabbit, 1:300 dilution), α-MLH1 (rabbit, 1:200 dilution), α-J3 (mouse, 1:500 dilution), and α-HEI10 (chicken, 1:1000, rabbit, 1:500 dilution). For ASY1, RAD51 and MLH1, microscopy was performed using a DeltaVision personal DV microscope (Applied precision/GE Healthcare) equipped with a CCD Coolsnap HQ2 camera (Photometrics). Images were captured and analyzed using SoftWoRx software version 5.5 (Applied precision/GE Healthcare). For ASY1 and RAD51 co-immunostaining of leptotene-stage nuclei, individual cell images were acquired as *Z*-stacks of 10 optical sections of 0.2 μm each, and the maximum intensity projection for each cell was determined using ImageJ. Numbers of MLH1 foci per cell and RAD51 foci per cell associated with ASY1 were counted manually. Wilcoxon tests were used to assess significant differences between genotypes for MLH1 and RAD51 foci counts.

Immunolocalization of MLH1 was performed on 3D-preserved meiocytes as previously described[67] with the following modifications: 5–10 flower buds were used for a single gel pad and were digested for 20 min at 37°C after fixation in a digestion mix of 0.3% (w/v) pectolyase Y-23 (MP Biomedicals), 0.3% (w/v) Driselase (Sigma), and 0.3% (w/v) Cellulase Onozuka R10 (Duchefa). The gel pads were mounted in Vectashield (Vectorlabs), and primary antibodies were incubated for 48–72 h. After treatment with primary and secondary antibodies, gels were washed four times in PBS with 0.1% Triton for 30 min. Scondary antibodies were diluted 1:250. Primary antibodies were rabbit α-MLH1 (1:500)[66], chicken α-HEI10 (1:10,000)[16], and rat α-ZYP1 (1:250)[68]. Secondary antibodies were conjugated with Alexa 488, Alexa 568 or Alexa 647 (Thermo Fisher Scientific). Observations were made using either a Zeiss AxioImager 2 microscope or a Leica confocal microscope TCS SP8 AOBS (Acousto-Optical Beam Splitter). On the Zeiss AxioImager 2 microscope, observations were made using a 60×/1.42 oil objective lens with 1.59 auxiliary magnification, and images were captured with a Zeiss AxioCam MR camera driven by Axiovision 4.7 at 0.24 μm intervals along the z-axis. On the Leica SP8 system, the images were acquired as previously

described[69], but using an HC PL APO CS2 63×/1.4 NA immersion objective lens. Fluorescent signals were recorded using LASX software in the Lightning mode. Z-stacks at 0.13 μm intervals were acquired and deconvolved using Lightning default parameters and the adaptative-vectashield option. All images were further processed using Imaris software (https://www.oxinst.com/).

For HEI10 and ZYP1 immunostaining in late-pachytene nuclei, 3D-structed illumination microscopy (3D-SIM) was performed using a Zeiss Elyra PS1 microscope as described by Morgan et al.[18]. Individual bivalents were traced using the SNT Fiji plugin. Trace fluorescence intensity quantification and HEI10 peak identification were performed using the bespoke image-analysis pipeline described in Morgan et al.[18]. Late-pachytene data was collected from 120 bivalents from 24 nuclei from four *hcr3* plants and 135 bivalents from 27 nuclei from four Col plants. The peak detection algorithm encountered problems for three *hcr3* bivalents and one Col bivalent, which were excluded from downstream data analysis.

Mathematical modelling

Simulations of the "coarsening model" for crossover patterning were performed as described in Morgan et al.[18]. For Col simulations, parameter values were identical to those used in wild-type simulations from Morgan et al.[18]. For *hcr3* simulations, all parameter values were fixed except for those parameters specifying the initial concentrations of HEI10, both on the synaptonemal complex and at recombination intermediates, which were each increased to be 1.3 times wild-type levels.

Yeast two hybrid (Y2H) assay

Y2H assay was performed as described by Nageswaran et al.[24]. The open reading frames of *J3* except J-domain and meiotic genes were cloned into pGBKT7 BD and pGADT7 AD vectors (Clontech, 630490) using BamHI and StuI sites, using a Gibson assembly cloning system (NEB E2621L). Plasmids of cloned BD and AD vectors were co-transformed into *S. cerevisiae* strain AH109 and selected on synthetic dropout medium lacking leucine (−L) and tryptophan (−T). The colonies of yeast transformant cells were streaked

onto both (−LT) and (−LTH (histidine) A (adenine)) synthetic media and grown for 3–5 d at 30 °C. The cells grown in synthetic medium (−LT) were grown until OD_{600} = 1 and diluted 10-, 100- and 1,000-fold in water and spotted on synthetic medium (−LTHA) for 3–7 d.

Co-immunoprecipitation analysis and proximity label assay using *Arabidopsis* protoplast transient expression

Arabidopsis protoplasts and plasmid DNA were prepared and co-immunoprecipitation analysis was performed as described by Nageswaran et al.[24]. Furthermore, 40 μg of epitope Myc- and HA-tagged DNA plasmids were co-transfected into approximately 20×10^3 protoplasts or separately transfected as a negative control and incubated for 6–12 h at room temperature (20°C). Protoplasts were centrifuged, harvested and total protein was extracted using extraction buffer (50 mM Tris-HCl pH 7.5, 100 mM NaCl, 5 mM EDTA, 1 mM dithiothreitol, protease inhibitor cocktail (Roche) and 1% Triton X-100). The isolated proteins were separated by SDS–PAGE using 8% polyacrylamide gels, transferred to a nitrocellulose membrane and detected with anti-HA (1:2,000 Roche 12013819001) or anti-Myc (1:2,000 Santa Cruz, sc-40) antibodies. For co-immunoprecipitation analysis, transfected protoplasts were lysed with IP buffer (50 mM Tris-HCl pH 7.5, 100 mM NaCl, 1 mM EDTA, 0.5% Triton X-100, 10% glycerol and protease inhibitor cocktail). Lysates were incubated with 1 μg anti-HA antibody for 12 h with rotation at 4 °C. The protoplast lysate and antibody mixture were incubated with Dynabeads Protein G (Invitrogen, 10004D) for an additional 2 h. Protein-coated Dynabeads were washed with IP buffer three times. Proteins were extracted using an extraction buffer and analyzed by immunoblotting using anti-Myc antibodies.

For TurboID-based proximity label assay, transfected protoplasts were incubated with biotin (5μM) for 1 h and lysed with IP buffer. Lysates were incubated with Dynabeads MyOne Streptavidin C1 (Invitrogen, 65001) in the equilibration buffer (50 mM Tris pH 7.5, 150 mM NaCl, 0.05% Triton-X-100, 1 mM DTT) over night at 4°C on a rotor wheel. The beads were washed with wash buffer 1 (50 mM Hepes pH 7.5, 500 mM NaCl, 1 mM EDTA, 1% Tri- ton-X-100, 0.5% Na-deoxycholate), wash buffer 2 (10 mM Tris pH 8,

250 mM LiCl, 1 mM EDTA, 0.5% NP-40, 0.5% Na-deoxycholate), and wash buffer 3 (50 mM Tris pH 7.5, 50 mM NaCl, 0.1% NP-40). Proteins were eluted by boiling the beads for 15 min at 98°C in elution buffer (10 mM Tris pH 7.5, 2% SDS, 5% beta mercaptoethanol, 2 mM biotin) and used for immunoblotting.

Immunoblot analysis of meiotic proteins in *Arabidopsis*

Approximately 0.1 g of floral buds smaller than approximately 0.6 mm were sampled and liquid nitrogen was used to grind the unopen buds with a mortar and pestle. Total protein was extracted using an extraction buffer (50 mM Tris-HCl pH 7.5, 100 mM NaCl, 5 mM EDTA, 1 mM dithiothreitol, protease inhibitor cocktail (Roche) and 1% Triton X-100). Extracted proteins were separated by SDS–PAGE using 8–12% polyacrylamide gels and transferred to PVDF membranes (Immobilon-P, Merck Millipore). The epitope tagged proteins were detected using anti-HA (1:2,000 Roche 12013819001) or anti-Myc (1:2,000 Santa Cruz sc-40) antibodies. For HEI10 immunoblot analysis, Western BLoT Blocking Buffer (T7131A, Takara, Japan) was added to the transferred membrane and incubated on the shaker at 20°C for 60 min. The membranes were washed using 1x PBS-T and then incubated with chicken anti-HEI10 antibody (1:1000 dilution, Institut Jean-Pierre Bourgin, France) at 4 °C overnight. After washing 3 times, the membranes were incubated with horseradish peroxidase (HRP)-conjugated goat anti-chicken IgY (1:2000 dilution, Abcam Ab97135) for 1 h at 20°C. The signals were detected using chemiluminescence with secondary horseradish peroxidase-conjugated antibodies (Clarity Western ECL, Bio-rad). Ponceau S staining of the membrane was used and shown for a loading control.

To detect ubiquitin- or SUMO-conjugated HEI10-Myc proteins, total protein was extracted from unopen flower buds smaller than approximately 0.6 mm of 6-week-old *pHEI10:HEI10-Myc* and *hcr3 pHEI10:HEI10-Myc* using lysis buffer (25mM HEPES, 5mM EDTA, 2% SDS and 1x protease inhibitor cocktail). Protein concentration was determined by bicinchoninic acid assay (Thermo Scientific, 23225). For immunoprecipitation of HEI10-Myc, 5 mg of protein lysates were incubated with 4 μg anti-Myc (Santa Cruz, sc-9E10) in IP buffer (50 mM Tris-HCl pH 7.5, 100 mM NaCl, 1 mM EDTA, 0.5% Triton X-100,

10% glycerol and protease inhibitor cocktail) for 12 h at 4°C. The lysate and antibody mixture were incubated with Dynabeads Protein G (Invitrogen, 10004D) for 2 h at 4°C, and Dynabeads were washed with IP buffer three times. Anti-K48-linkage specific polyubiquitin (CellSignaling 12805), anti-SUMO1 (Abcam ab5316), and anti-Myc (Santa Cruz, sc-40 HRP) antibodies were used to detect modified HEI10-Myc proteins for immunoblot analysis. For reprobing immunoblot, the membrane was incubated in stripping buffer (62.5 Tris-HCl pH 6.8, 0.5% SDS, 0.8% beta mercaptoethanol) for 40 min at 50°C.

Data availability

Seeds of *Arabidopsis* transgenic plants used for this study are freely available on request. GBS data in this study are available in the ArrayExpress database at EMBL-EBL (http://www.ebi.ac.uk/arrayexpress) under the accession numbers E-MTAB-10168, E-MTAB-11586, E-MTAB-12663, E-MTAB-12692, E-MTAB-12694, E-MTAB-12695, E-MTAB-12696, E-MTAB-12697, E-MTAB-12726, and E-MTAB-13412–13415. RNA-seq data have been deposited at EMBL-EBI under accession number E-MTAB-12699 and E-MTAB-13417.

Code availability

All custom code involved in the manuscript are available at https://github.com/KyuhaChoi-Lab/HCR3

References

1. Villeneuve, A. M. & Hillers, K. J. Whence meiosis? *Cell* **106**, 647–50 (2001).

2. Hunter, N. Meiotic recombination: The essence of heredity. *Cold Spring Harb. Perspect. Biol.* **7**, 1–36 (2015).

3. Mercier, R., Mézard, C., Jenczewski, E., Macaisne, N. & Grelon, M. The Molecular Biology of Meiosis in Plants. *Annu. Rev. Plant Biol.* **66**, 297–327 (2015).

4. Pyatnitskaya, A., Borde, V. & De Muyt, A. Crossing and zipping: molecular duties of the ZMM proteins in meiosis. *Chromosoma* **128**, 181–198 (2019).

5. Berchowitz, L. E. & Copenhaver, G. P. Genetic interference: don't stand so close to me. *Curr. Genomics* **11**, 91–102 (2010).

6. Berchowitz, L. E., Francis, K. E., Bey, A. L. & Copenhaver, G. P. The Role of AtMUS81 in Interference-Insensitive Crossovers in A. thaliana. *PLoS Genet.* **3**, e132 (2007).

7. Crismani, W. *et al.* FANCM Limits Meiotic Crossovers. *Science* **336**, 1588–1590 (2012).

8. Séguéla-Arnaud, M. *et al.* Multiple mechanisms limit meiotic crossovers: TOP3α and two BLM homologs antagonize crossovers in parallel to FANCM. *Proc. Natl. Acad. Sci. U. S. A.* **112**, 4713–4718 (2015).

9. Agarwal, S. & Roeder, G. S. Zip3 provides a link between recombination enzymes and synaptonemal complex proteins. *Cell* **102**, 245–255 (2000).

10. De Muyt, A. *et al.* E3 ligase Hei10: A multifaceted structure-based signaling molecule with roles within and beyond meiosis. *Genes Dev.* **28**, 1111–1123 (2014).

11. Ziolkowski, P. A. *et al.* Natural variation and dosage of the HEI10 meiotic E3 ligase control Arabidopsis crossover recombination. *Genes Dev.* **31**, 306–317 (2017).

12. Qiao, H. *et al.* Antagonistic roles of ubiquitin ligase HEI10 and SUMO ligase RNF212 regulate meiotic recombination. *Nat. Genet.* **46**, 194–199 (2014).

13. Reynolds, A. *et al.* RNF212 is a dosage-sensitive regulator of crossing-over during mammalian meiosis. *Nat. Genet.* **45**, 269–278 (2013).

14. Bhalla, N., Wynne, D. J., Jantsch, V. & Dernburg, A. F. ZHP-3 acts at crossovers to couple meiotic recombination with synaptonemal complex disassembly and bivalent formation in C. elegans. *PLoS Genet.* **4**, e1000235 (2008).

15. Serra, H. *et al.* Massive crossover elevation via combination of HEI10 and recq4a recq4b during Arabidopsis meiosis. *Proc. Natl. Acad. Sci. U. S. A.* **115**, 2437–2442 (2018).

16. Chelysheva, L. *et al.* The Arabidopsis HEI10 Is a New ZMM Protein Related to Zip3. *PLoS Genet.* **8**, e1002799 (2012).

17. Kong, A. *et al.* Sequence Variants in the RNF212 Gene Associate with Genome-Wide Recombination Rate. *Science* **319**, 1398–1401 (2008).

18. Morgan, C. *et al.* Diffusion-mediated HEI10 coarsening can explain meiotic crossover positioning in Arabidopsis. *Nat. Commun.* **12**, 4674 (2021).

19. Banani, S. F., Lee, H. O., Hyman, A. A. & Rosen, M. K. Biomolecular condensates: Organizers of cellular biochemistry. *Nat. Rev. Mol. Cell Biol.* **18**, 285–298 (2017).

20. France, M. G. *et al.* ZYP1 is required for obligate cross-over formation and cross-over interference in Arabidopsis. *Proc. Natl. Acad. Sci. U. S. A.* **118**, 1–11 (2021).

21. Capilla-Pérez, L. *et al.* The synaptonemal complex imposes crossover interference and heterochiasmy in Arabidopsis. *Proc. Natl. Acad. Sci. U. S. A.* **118**, 1–11 (2021).

22. Lambing, C., Kuo, P. C., Tock, A. J., Topp, S. D. & Henderson, I. R. ASY1 acts as a dosage-dependent antagonist of telomere-led recombination and mediates crossover interference in Arabidopsis. *Proc. Natl. Acad. Sci. U. S. A.* **24**, 13647–13658 (2020).

23. Zhang, L. *et al.* Topoisomerase II mediates meiotic crossover interference. *Nature* **511**, 551–556 (2014).

24. Nageswaran, D. C. *et al.* HIGH CROSSOVER RATE1 encodes PROTEIN PHOSPHATASE X1 and restricts meiotic crossovers in Arabidopsis. *Nat. Plants* **7**, 452–467 (2021).

25. Ahuja, J. S. *et al.* Control of meiotic pairing and recombination by chromosomally tethered 26 S proteasome. *Science* **355**, 408–411 (2017).

26. Haversat, J. *et al.* Robust designation of meiotic crossover sites by CDK-2 through phosphorylation of the MutSγ complex. *Proc. Natl. Acad. Sci. U. S. A.* **119**, e2117865119 (2022).

27. He, W. *et al.* Regulated Proteolysis of MutSγ Controls Meiotic Crossing Over. *Mol. Cell* **78**, 168-183.e5 (2020).

28. Cheng, C.-H. *et al.* SUMO modifications control assembly of synaptonemal complex and polycomplex in meiosis of Saccharomyces cerevisiae. *Genes Dev.* **20**, 2067–2081 (2006).

29. Bhagwat, N. R. *et al.* SUMO is a pervasive regulator of meiosis. *Elife* **10**, e57720 (2021).

30. He, W. *et al.* SUMO fosters assembly and functionality of the MutSγ complex to facilitate meiotic crossing over. *Dev. Cell* **56**, 2073-2088.e3 (2021).

31. Rao, H. B. D. P. *et al.* A SUMO-ubiquitin relay recruits proteasomes to chromosome axes to regulate meiotic recombination. *Science* **355**, 306–371 (2017).

32. Zhang, L. *et al.* Topoisomerase II mediates meiotic crossover interference. *Nature* **511**, 551–556 (2014).

33. Rosenzweig, R., Nillegoda, N. B., Mayer, M. P. & Bukau, B. The Hsp70 chaperone network. *Nature Reviews Molecular Cell Biology* **20**, 665–680 (2019).

34. Jiang, Y., Rossi, P. & Kalodimos, C. G. Structural basis for client recognition and activity of Hsp40 chaperones. *Science* **365**, 1313–1319 (2019).

35. Lee, D. H., Sherman, M. Y. & Goldberg, A. L. Involvement of the molecular chaperone Ydj1 in the ubiquitin-dependent degradation of short-lived and abnormal proteins in Saccharomyces cerevisiae. *Mol. Cell. Biol.* **16**, 4773–4781 (1996).

36. Mogk, A., Bukau, B. & Kampinga, H. H. Cellular Handling of Protein Aggregates by Disaggregation Machines. *Mol. Cell* **69**, 214–226 (2018).

37. Shen, L., Kang, Y. G. G., Liu, L. & Yu, H. The J-domain protein J3 mediates the integration of flowering signals in Arabidopsis. *Plant Cell* **23**, 499–514 (2011).

38. Barghetti, A. *et al.* Heat-shock protein 40 is the key farnesylation target in meristem size control, abscisic acid signaling, and drought resistance. *Genes Dev.* **31**, 2282–2295 (2017).

39. Kim, J. *et al.* Arabidopsis HEAT SHOCK FACTOR BINDING PROTEIN is required to limit meiotic crossovers and HEI10 transcription. *EMBO J.* **41**, e109958 (2022).

40. Rowan, B. A., Patel, V., Weigel, D. & Schneeberger, K. Rapid and inexpensive whole-genome genotyping-by-sequencing for crossover localization and fine-scale genetic mapping. *G3 Genes, Genomes, Genet.* **5**, 385–398 (2015).

41. Berchowitz, L. E. & Copenhaver, G. P. Fluorescent Arabidopsis tetrads: a visual assay for quickly developing large crossover and crossover interference data sets. *Nat. Protoc.* **3**, 41–50 (2008).

42. Modliszewski, J. L. *et al.* Elevated temperature increases meiotic crossover frequency via the interfering (Type I) pathway in Arabidopsis thaliana. *PLOS Genet.* **14**, e1007384 (2018).

43. Lloyd, A., Morgan, C., Franklin, C. & Bomblies, K. Plasticity of Meiotic Recombination Rates in Response to Temperature in Arabidopsis. *Genetics* **208**, 1409–1420 (2018).

44. Fang, N. N. *et al.* Rsp5/Nedd4 is the main ubiquitin ligase that targets cytosolic misfolded proteins following heat stress. *Nat. Cell Biol.* **16**, 1227–1237 (2014).

45. de Felippes, F. F., Wang, J. & Weigel, D. MIGS: miRNA-induced gene silencing. *Plant J.* **70**, 541–547 (2012).

46. McLoughlin, F., Kim, M., Marshall, R. S., Vierstra, R. D. & Vierling, E. HSP101 interacts with the proteasome and promotes the clearance of ubiquitylated protein aggregates. *Plant Physiol.* **180**, 1829–1847 (2019).

47. Yoo, H., Bard, J. A. M., Pilipenko, E. V. & Drummond, D. A. Chaperones directly and efficiently disperse stress-triggered biomolecular condensates. *Mol. Cell* **82**, 741-755.e11 (2022).

48. Prusicki, M. A. *et al.* Live cell imaging of meiosis in arabidopsis thaliana. *Elife* **8**, (2019).

49. Fozard, J. A., Morgan, C. & Howard, M. Coarsening dynamics can explain meiotic crossover patterning in both the presence and absence of the synaptonemal complex. *Elife* **12**, e79408 (2023).

50. Durand, S. *et al.* Joint control of meiotic crossover patterning by the synaptonemal complex and HEI10 dosage. *Nat. Commun.* **13**, (2022).

51. Morgan, C. *et al.* Evolution of crossover interference enables stable autopolyploidy by ensuring pairwise partner connections in Arabidopsis arenosa. *Curr. Biol.* **31**, 4713–4726 (2021).

52. Wu, G., Rossidivito, G., Hu, T., Berlyand, Y. & Poethig, R. S. Traffic lines: new tools for genetic analysis in Arabidopsis thaliana. *Genetics* **200**, 35–45 (2015).

53. Melamed-Bessudo, C., Yehuda, E., Stuitje, A. R. & Levy, A. A. A new seed-based assay for meiotic recombination in Arabidopsis thaliana. *Plant J.* **43**, 458–66 (2005).

54. Charng, Y. Y., Liu, H. C., Liu, N. Y., Hsu, F. C. & Ko, S. S. Arabidopsis Hsa32, a novel heat shock protein, is essential for acquired thermotolerance during long recovery after acclimation. *Plant Physiol.* **140**, 1297–1305 (2006).

55. Fernandes, J. B., Seguela-Arnaud, M., Larcheveque, C., Lloyd, A. H. & Mercier, R. Unleashing meiotic crossovers in hybrid plants. *Proc. Natl. Acad. Sci. U. S. A.* **115**, 2431–2436 (2017).

56. Schneeberger, K. *et al.* SHOREmap: Simultaneous mapping and mutation identification by deep sequencing. *Nature Methods* **6**, 550–551 (2009).

57. Schiml, S., Fauser, F. & Puchta, H. The CRISPR/Cas system can be used as nuclease for in planta gene targeting and as paired nickases for directed mutagenesis in Arabidopsis resulting in heritable progeny. *Plant J.* **80**, 1139–1150 (2014).

58. Mair, A., Xu, S. L., Branon, T. C., Ting, A. Y. & Bergmann, D. C. Proximity labeling of protein complexes and cell type specific organellar proteomes in Arabidopsis enabled by TurboID. *Elife* **8**, e47864 (2019).

59. van Tol, N., Rolloos, M., van Loon, P. & van der Zaal, B. J. MeioSeed: a CellProfiler-based program to count fluorescent seeds for crossover frequency analysis in Arabidopsis thaliana. *Plant Methods* **14**, 32 (2018).

60. Ziolkowski, P. A. *et al.* Juxtaposition of Heterozygous and Homozygous Regions Causes Reciprocal Crossover Remodelling via Interference During Arabidopsis Meiosis. *Elife* **4**, e03708 (2015).

61. Lim, E. C. *et al.* DeepTetrad: high-throughput image analysis of meiotic tetrads by deep learning in Arabidopsis thaliana. *Plant J.* **101**, 473–483 (2020).

62. Choi, K. *et al.* Nucleosomes and DNA methylation shape meiotic DSB frequency in Arabidopsis thaliana transposons and gene regulatory regions. *Genome Res.* **28**, 532–546 (2018).

63. Liao, Y., Smyth, G. K. & Shi, W. FeatureCounts: An efficient general purpose program for assigning sequence reads to genomic features. *Bioinformatics* **30**, 923–930 (2014).

64. Love, M. I., Huber, W. & Anders, S. Moderated estimation of fold change and dispersion for RNA-seq data with DESeq2. *Genome Biol.* **15**, 550 (2014).

65. Walker, J. *et al.* Sexual-lineage-specific DNA methylation regulates meiosis in Arabidopsis. *Nat. Genet.* **50**, 130–137 (2018).

66. Chelysheva, L. *et al.* An easy protocol for studying chromatin and recombination protein dynamics during Arabidopsis thaliana meiosis: immunodetection of cohesins, histones and MLH1. *Cytogenet. Genome Res.* **129**, 143–53 (2010).

67. Hurel, A. *et al.* A cytological approach to studying meiotic recombination and chromosome dynamics in *Arabidopsis thaliana* male meiocytes in three dimensions. *Plant J.* **95**, 385–396 (2018).

68. Higgins, J. D., Sanchez-Moran, E., Armstrong, S. J., Jones, G. H. & Franklin, F. C. H. The Arabidopsis synaptonemal complex protein ZYP1 is required for chromosome synapsis and normal fidelity of crossing over. *Genes Dev.* **19**, 2488–2500 (2005).

69. Vrielynck, N. *et al.* Conservation and divergence of meiotic DNA double strand break forming mechanisms in Arabidopsis thaliana. *Nucleic Acids Res.* **49**, 9821–9835 (2021).

Acknowledgments

We thank Gregory Copenhaver (University of North Carolina at Chapel Hill), Abraham Levy (The Weizmann Institute of Science), and Scott Poethig (University of Pennsylvania) for providing CTLs/FTLs. We thank Chris Franklin (University of Birmingham) for providing ASY1 and RAD51 antibodies. We appreciate the support of IJPB's plant observatory technological platforms.

Author contributions: HK, JK, CM, IR and KC designed the study. HK, JK, NS, CL, CM, AC, DB, JP, YL, YMP, JG, AH, PK and KC performed experiments. HK, JK, NS, CL, CM, AC, DB, JP, YL, YMP, JAF, PK, MH, MG, IRH and KC analyzed the results. HK, JK and KC wrote the paper, with review and editing by all authors.

Funding: This work was supported by Suh Kyungbae Foundation SUHF-17020079, Samsung Science and Technology Foundation SSTF-BA2202-09, Next-Generation BioGreen 21 Program PJ01337001 and National Research Foundation of Korea NRF-2020R1A2C2007763 to KC; National Research Foundation of Korea NRF-2021R1A6A3A01087206 to JK; Agence Nationale de la Recherche CO-PATT-ANR-20-CE12-0006 and Saclay Plant Sciences-SPS ANR-17-EUR-0007 to MG; BBSRC grants BB/S006842/1, BB/S020012/1 and BB/V003984/1 to IRH; European Research Council Consolidator Award ERC-2015-CoG-681987 to CL and IRH; BBSRC grant BB/X011003/1 to CL; BBSRC Discovery Fellowship BB/V005774/1 to CM; BBSRC Institute Strategic Programme GEN BB/P013511/1 to MH

Competing Interests Declaration: Authors declare that they have no competing interests.

Supplementary Tables

Supplementary Table 1. *420* crossover frequency (cM) in wild type (Col), *hcr3*, *hcr3/+* and high recombination *hcr3* BC_1F_2 individuals

Supplementary Table 2. *420* crossover frequency (cM) in wild type (Col), *j3-1/+*, *j3-1*, *j3-3* and *J3::Myc-J3 j3-1* transgenic lines

Supplementary Table 3. Pollen tetrad FTL crossover frequency (cM) of *I1bc* and *I3bc* in wild type (Col), *j3-1* and *j3-3*

Supplementary Table 4. Pollen tetrad FTL crossover frequency (cM) of *I1bc* and *I3bc* in wild type (Col) and *j2-2*

Supplementary Table 5. Crossover frequency (cM) of fluorescent seed reporter lines (CTLs) in wild type (Col), *j3-1* and *j3-3*

Supplementary Table 6. *420* crossover frequency (cM) in wild type (Col), *J3::J3, J3::J3*^{G155R}, *DMC1::J3* and *DMC1::J3*^{G155R} transgenic lines

Supplementary Table 7. *CTL5.14* crossover frequency (cM) in wild type (Col), *hcr3*, and transgenic lines expressing *J3* or $J3^{G155R}$ under the different promoters

Supplementary Table 8. *420* crossover frequency (cM) in wild type (Col), *j3-1*, *j3-1 j2-2/+*, *j3-3*, *j2-2*, and *j3-1/+ j2-2* mutant lines

Supplementary Table 9. *420* crossover frequency (cM) in wild type (Col), *hcr3*, *j3-1*, *j3-1 J3::HA-J2*, *j3-1 meiMIGS-J2*, and transgenic lines expressing $J2^{G156R}$ under different meiotic gene promoters

Supplementary Table 10. Crossover frequency (cM) of fluorescent seed reporter lines (CTLs) in wild type (Col) and *hcr3*

Supplementary Table 11. Pollen tetrad FTL crossover frequency (cM), interference ratio (IFR), more than double crossover (DCO) ratio of *I1bc*, *I3bc* and *I5ab* in wild type (Col) and *hcr3*

Supplementary Table 12. *420* crossover frequency (cM) of male and female meiosis in wild type (Col), *hcr3* and $J3::J3^{G155R}$ transgenic lines

Supplementary Table 13. Crossover frequency (cM) of fluorescent seed reporter lines (CTLs) in wild type, $J3::J3^{G155R}$ Col×L*er*, $SPO11\text{-}1::J3^{G155R}$ Col×L*er*, and *j3-1/j3-5* F_1 hybrid plants

Supplementary Table 14. Crossover numbers identified by sequencing Col×L*er*, $J3::J3^{G155R}$ Col×L*er*, $SPO11\text{-}1::J3^{G155R}$ Col×L*er*, and *j3-1* × *j3-5* F_2 populations

Supplementary Table 15. Crossover numbers of male and female meiosis identified by sequencing in Col×L*er* and $J3::J3^{G155R}$ Col×L*er* male and female F_1 populations

Supplementary Table 16. Crossover numbers identified by sequencing *recq4a recq4b* Col×L*er* and *recq4a recq4b* $J3::J3^{G155R}$ Col×L*er* F_2 populations

Supplementary Table 17. *420* crossover frequency (cM) in wild type (Col), *hcr3*, *fancm*, *hcr3 fancm*, *hei10*, *hcr3 hei10*, *zip4* and *hcr3 zip4*

Supplementary Table 18. Pollen tetrad FTL crossover frequency (cM) of *I3bc* in wild type (Col), *hcr3*, *recq4a recq4b* and *hcr3 recq4a recq4b*

Supplementary Table 19. Pollen tetrad FTL crossover frequency (cM) of *I1bc* in wild type (Col), *mus81*, *hcr3* and *hcr3 mus81*

Supplementary Table 20. Pollen tetrad FTL crossover frequency (cM) of *I3bc* and *I5ab* in wild type (Col) and *hcr3* grown in high temperature

Supplementary Table 21. Pollen viability in Col, *hcr3*, L*er*, and *j3* alleles

Supplementary Table 22. RAD51 foci number per cell in wild type (Col) and *hcr3*

Supplementary Table 23. MLH1 foci number per cell in wild type (Col), *hcr3*, *j3-1*, and *j3-3*

Supplementary Table 24. Analysis of double crossovers of male and female meiosis identified by sequencing in Col×L*er* and *J3::J3*^{G155R} Col×L*er* male and female F_1 populations

Supplementary Table 25. Yeast two hybrid analysis of interactions between J3 or J3^{G155R} with meiotic proteins

Supplementary Table 26. Crossover frequency (cM) of fluorescent seed reporter lines (CTLs) in wild-type (Col), *meiMIGS-HSP70-1*, and *meiMIGS-HSP70-3* transgenic lines

Supplementary Table 27. *CTL1.26* crossover frequency (cM) in wild type (Col), *hcr1*, *hcr3* and *hcr1 hcr3*

Supplementary Table 28. List of oligonucleotides used in this study

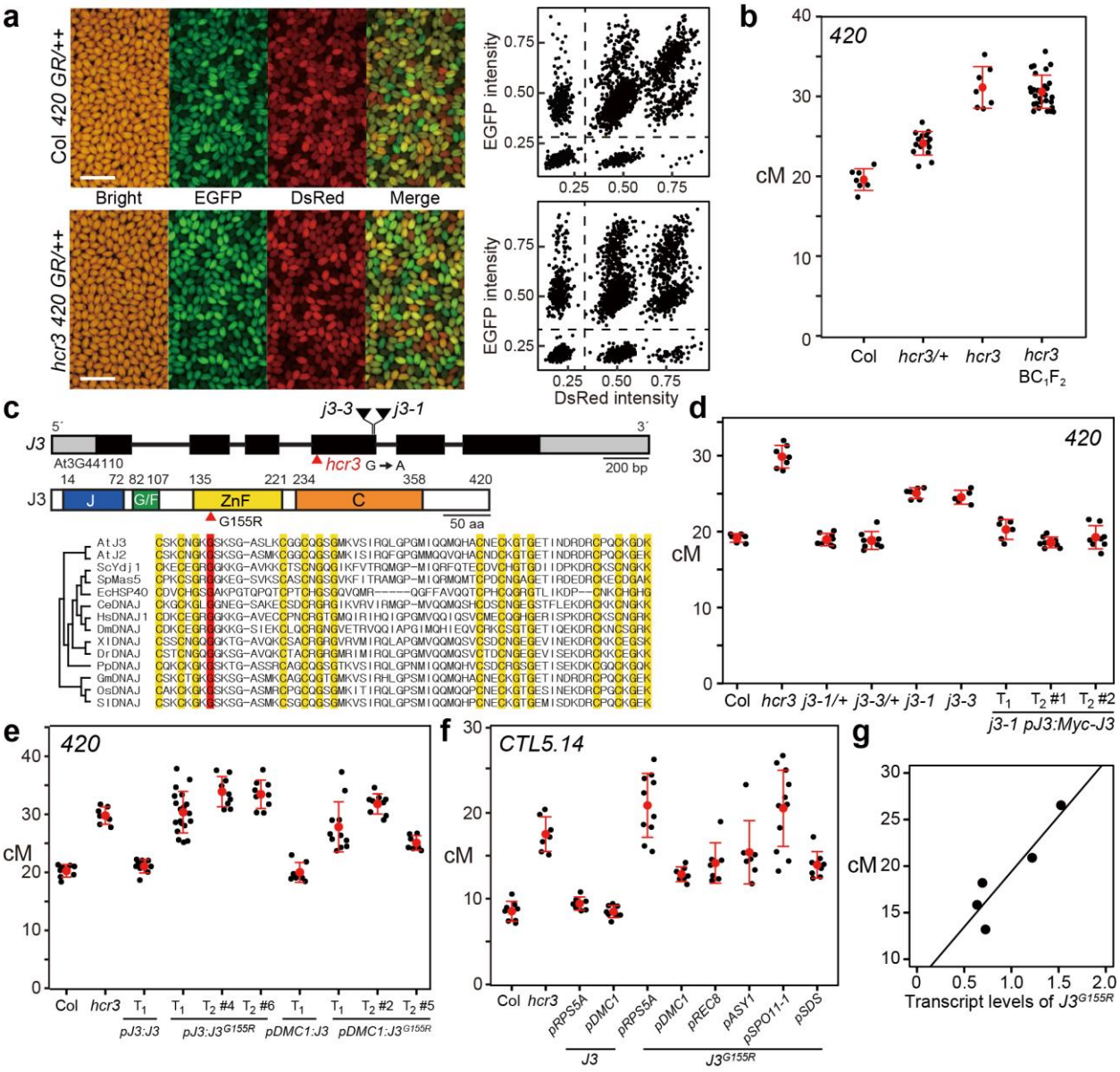

Fig. 1. Isolation of *hcr3* as a dominant-negative *j3* mutant. a, Representative images of fluorescent seed crossover reporter *420* in wild-type Col and *hcr3*. **b,** *420* crossover frequency (cM) in Col, *hcr3*/+, *hcr3*, and *hcr3* BC_1F_2 plants. **c,** *hcr3* mutation and *J3* and J3 secondary structure. Exons are presented as boxes (black, coding sequence; gray, untranslated regions) and introns as lines. The red arrow indicates the G-to-A substitution site of *hcr3*. The ZnF regions of J3 orthologs from diverse eukaryotes are shown with a phylogenetic tree. **d,** *420* crossover frequency (cM) in *j3* recessive mutants and complementation analysis. **e,** Increased *420* crossover frequencies (cM) in transgenic plants expressing $J3^{G155R}$. **f,** As in **(e)**, but showing *CTL5.14* crossover frequencies using different meiotic gene promoters. **g,** Correlation between crossover frequencies (cM) and $J3^{G155R}$ transcript levels in *SPO11-1::J3*^{G155R} transgenic plants. **(b, d** to **f)** Black dots indicate cM values of individual plants. Red dots and horizontal lines represent mean ± s.d. of cM values from individual plants (one-sided Welch's t-test). $n \geq 6$ plants of biological replicates.

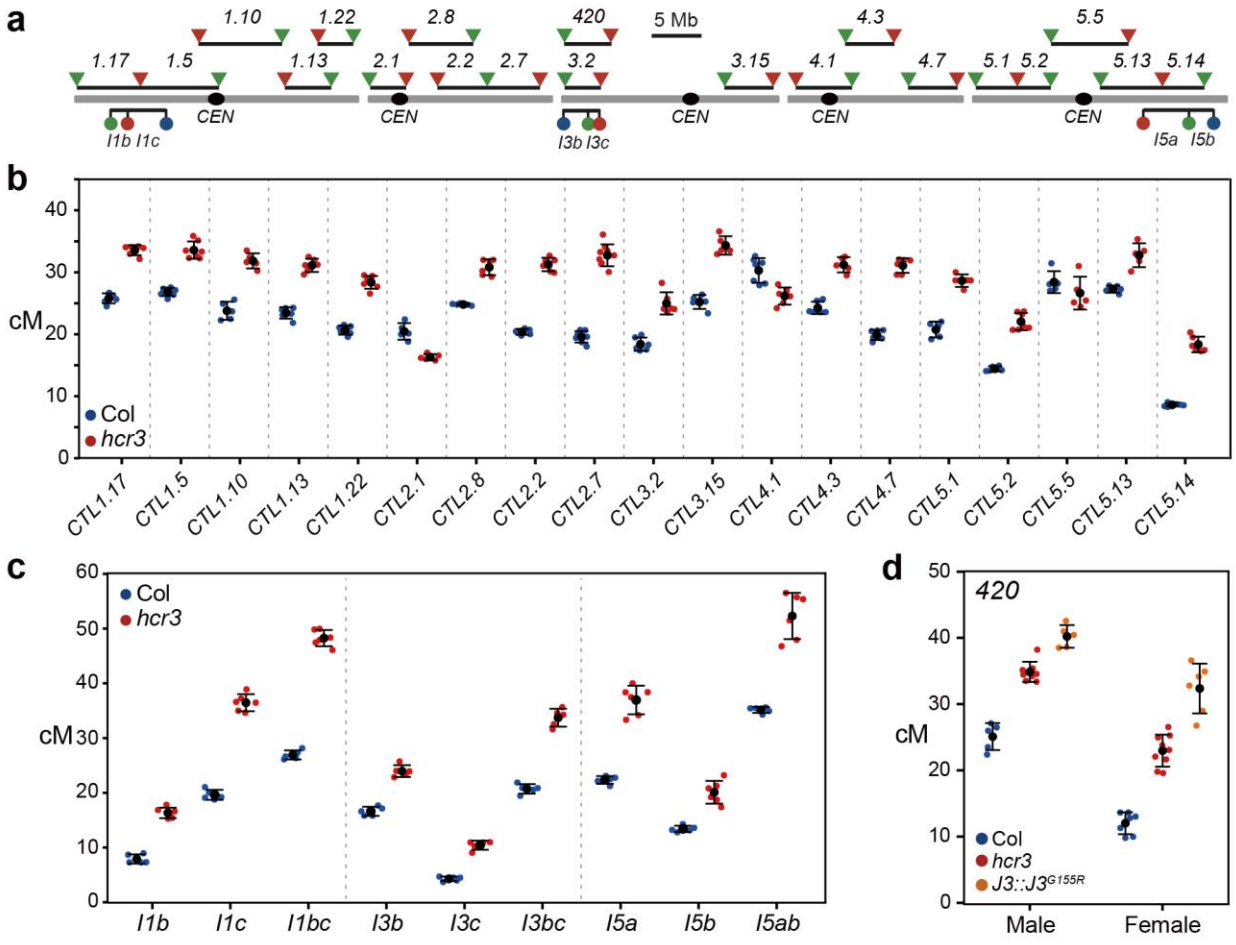

Fig. 2. Increased crossover frequencies in chromosome arms in *hcr3* and *J3::J3*^{G155R} plants. a, Seed (triangles) and pollen (circles) FTLs throughout the *Arabidopsis* genome. Lines represent the interval positions. **b,** Crossover frequencies of seed FTL/CTL lines in Col (blue) and *hcr3* (red). **c,** As for (**b**), but showing crossover frequencies of pollen FTL lines. **d,** Crossover frequencies of *420* interval in Col (blue), *hcr3* (red) and *J3::J3*^{G155R} (orange) for male and female meiosis. **(b– d)** Blue, red and orange dots indicate cM values of individual plants. Mean ± s.d. of cM values from individual plants are indicated by black dots and horizontal lines (one-sided Welch's t-test). $n \geq 6$ plants of biological replicates.

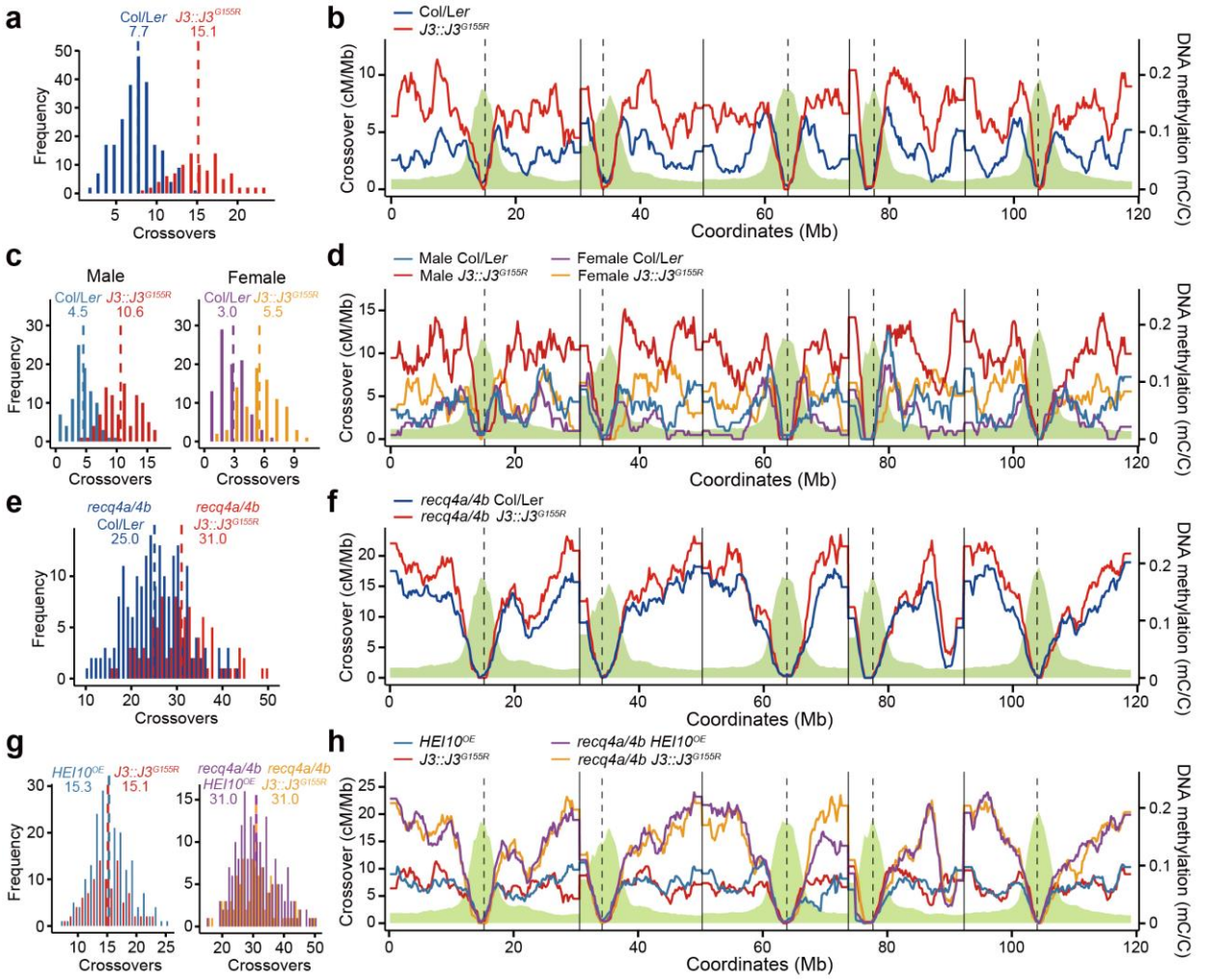

Fig. 3. *J3*^{G155R} expression increases crossovers in a hybrid context. a and **b**, Histograms of sex-averaged crossover number (**a**) and genomic crossover landscapes (**b**) in Col×L*er* (blue, *n* = 240) and *J3::J3*^{G155R} Col×L*er* (red, *n* = 96) F_2 individuals. **c** and **d,** As in (**a** and **b**), but showing analysis from male (blue, Col×L*er*, *n* = 96; red, *J3::J3*^{G155R} Col×L*er*, *n* = 96) and female (purple, Col×L*er*, *n* = 95; orange, *J3::J3*^{G155R} Col×L*er*, *n* = 90) meiosis. **e** and **f,** As in (**a** and **b**), but showing analysis from a *recq4a recq4b* background (blue, *recq4a recq4b* Col×Ler, *n* = 151; red, *recq4a recq4b J3::J3*^{G155R} Col×Ler, *n* = 96). (**a, c, e, g**) Significance between genotypes was tested by Welch's tests. (**b, d, f, h**) Green indicates DNA methylation levels along chromosomes. Vertical solid and dashed lines represent telomeres and centromeres, respectively.

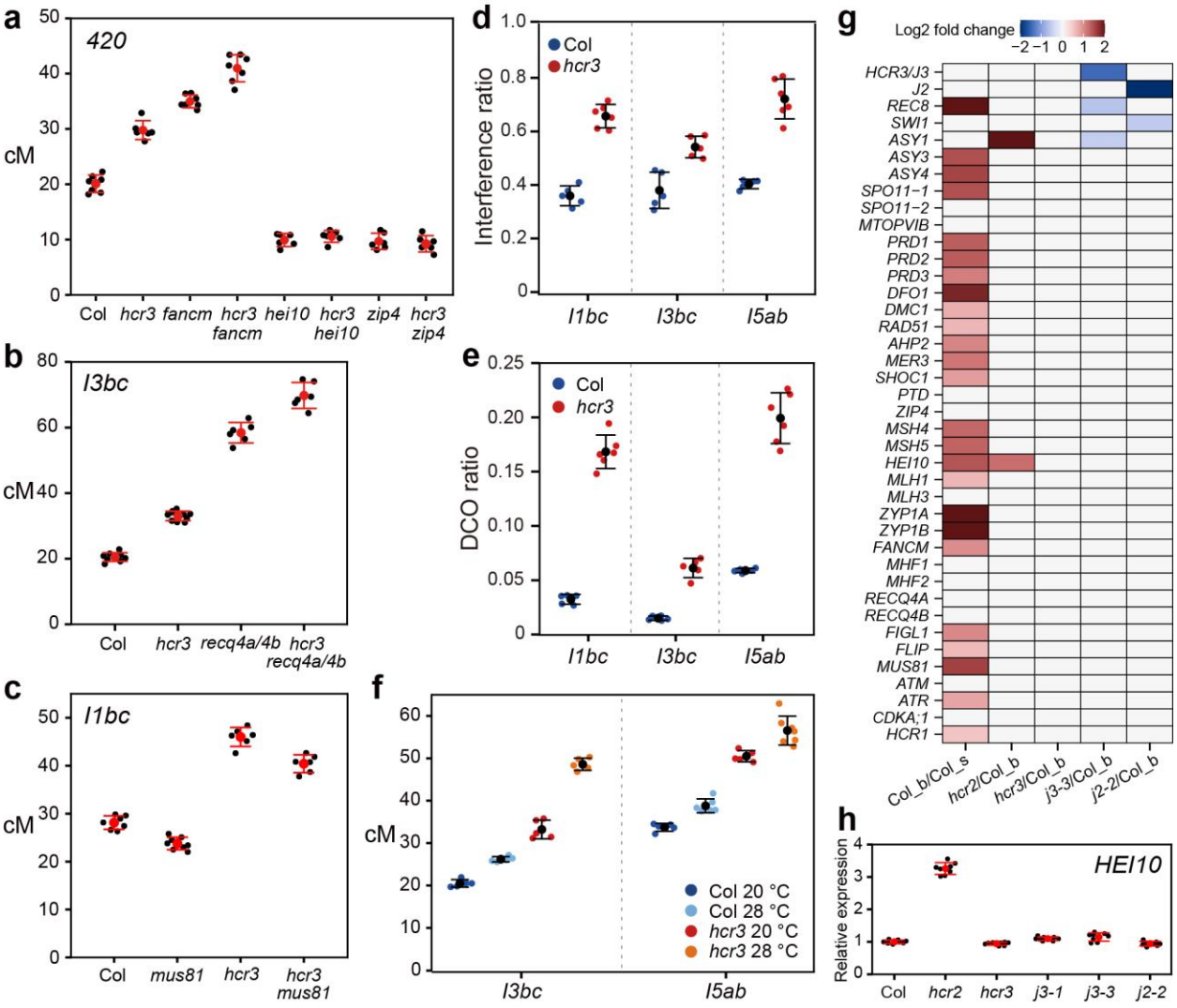

Fig. 4. *hcr3* increases interfering crossovers and reduces interference. a, *420* crossover frequencies in Col, *hcr3*, *fancm*, *hei10*, *zip4* and combinations of *hcr3* in *fancm*, *hei10*, and *zip4*. **b,** *I3bc* crossover frequencies in Col, *hcr3*, *recq4a recq4b*, and *hcr3 recq4a recq4b*. **c,** *I1bc* crossover frequencies in Col, *mus81*, *hcr3*, and *hcr3 mus81*. **d** and **e,** Crossover interference ratio (**d**) and double crossover (DCO) ratios (**e**) in FTL pollen tetrads in Col (blue) and *hcr3* (red). **f,** *420* crossover frequencies in Col and *hcr3* grown in optimal and high temperatures. **g,** Heatmap representation of transcript levels and fold changes for meiotic recombination genes in Col seedlings (s), Col flower buds (b), *hcr2*, *hcr3*, *j3-3*, and *j2-2* flower buds from RNA-seq data. **h,** RT-qPCR analysis of *HEI10* in Col, *hcr2*, *hcr3*, *j3-1*, *j3-3*, and *j2-2* male meiocytes. Data points (black) indicate two or three technical duplicates of three biological replicates. Red dots and horizontal lines indicate mean ± s.d. values (one-sided Welch's *t*-test). Red (**a, b, c**) or black (**d, e, f**) dots and horizontal lines indicate mean ± s.d. of cM values from individual plants (one-sided Welch's t-test). Black (**a, b, c**) and colored (**d, e, f**) dots represent cM values of individual plants. $n \geq 5$ plants of biological replicates.

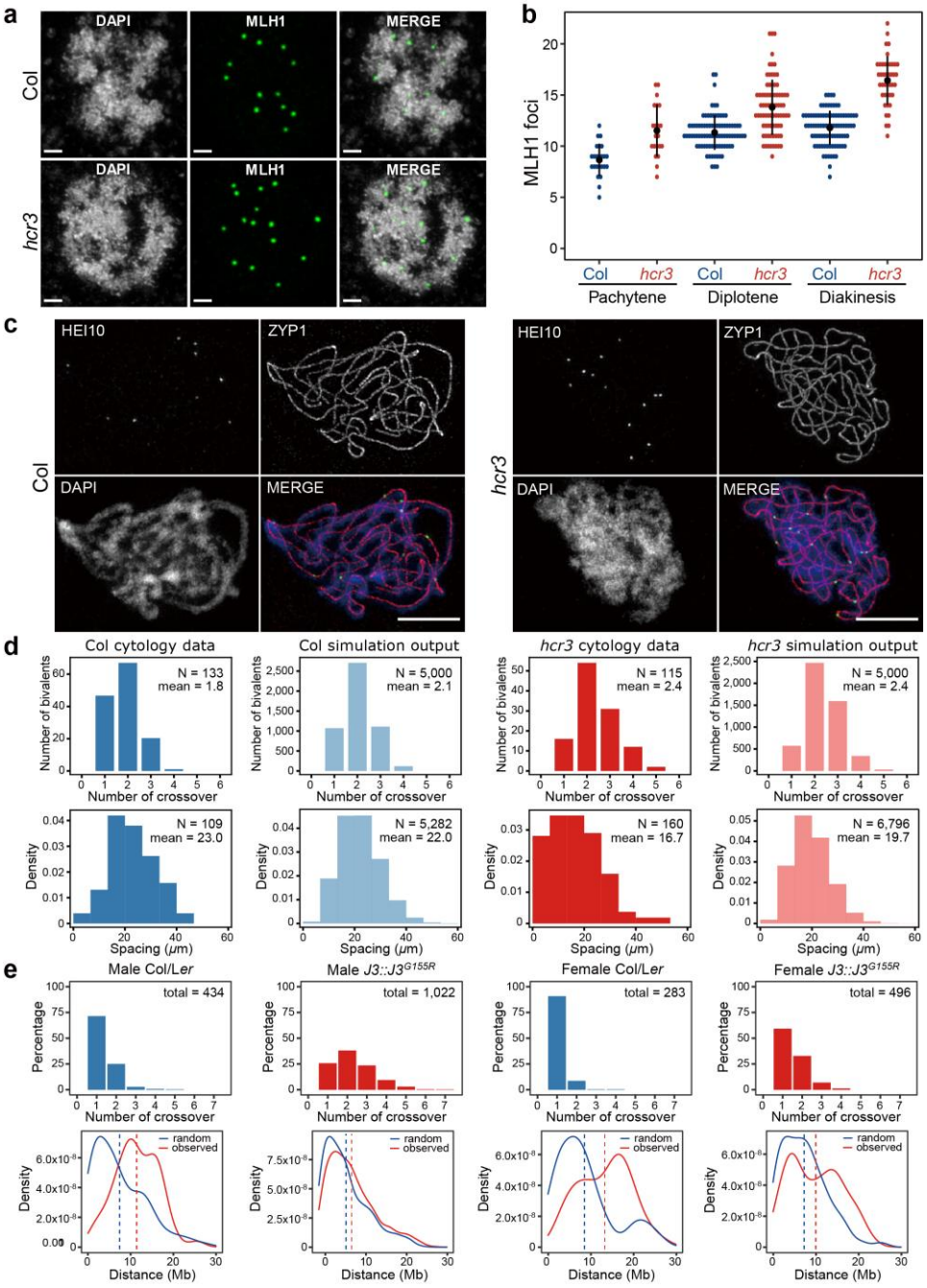

Fig. 5. *hcr3* elevates interfering crossovers and closely-spaced crossovers per bivalent. a, Representative images of immunostained MLH1 foci at diakenasis stage in three-dimension preserved Col and *hcr3* male meiocytes. Nuclear DNA was stained with DAPI (white). Scale bar = 5μm. **b,** Quantification of immunostained MLH1 foci at pachytene, diplotene, and diakinesis stages in Col and *hcr3*. **c,** Representative images of immunostained HEI10 foci and ZYP1 in Col and *hcr3* at late-pachytene stage. Scale bar = 5μm. **d,** Comparison of late-pachytene cytological data and coarsening model simulation output showing the number of crossover per bivalent and the distribution of spacing between adjacent crossovers in Col and *hcr3*. **e,** Genotyping-by-sequencing analysis of plots showing the number of crossovers and inter-crossover distance per chromatid in Col×Ler and *J3::J3*^{G155R} Col×Ler F_1 hybrid male and female meiosis.

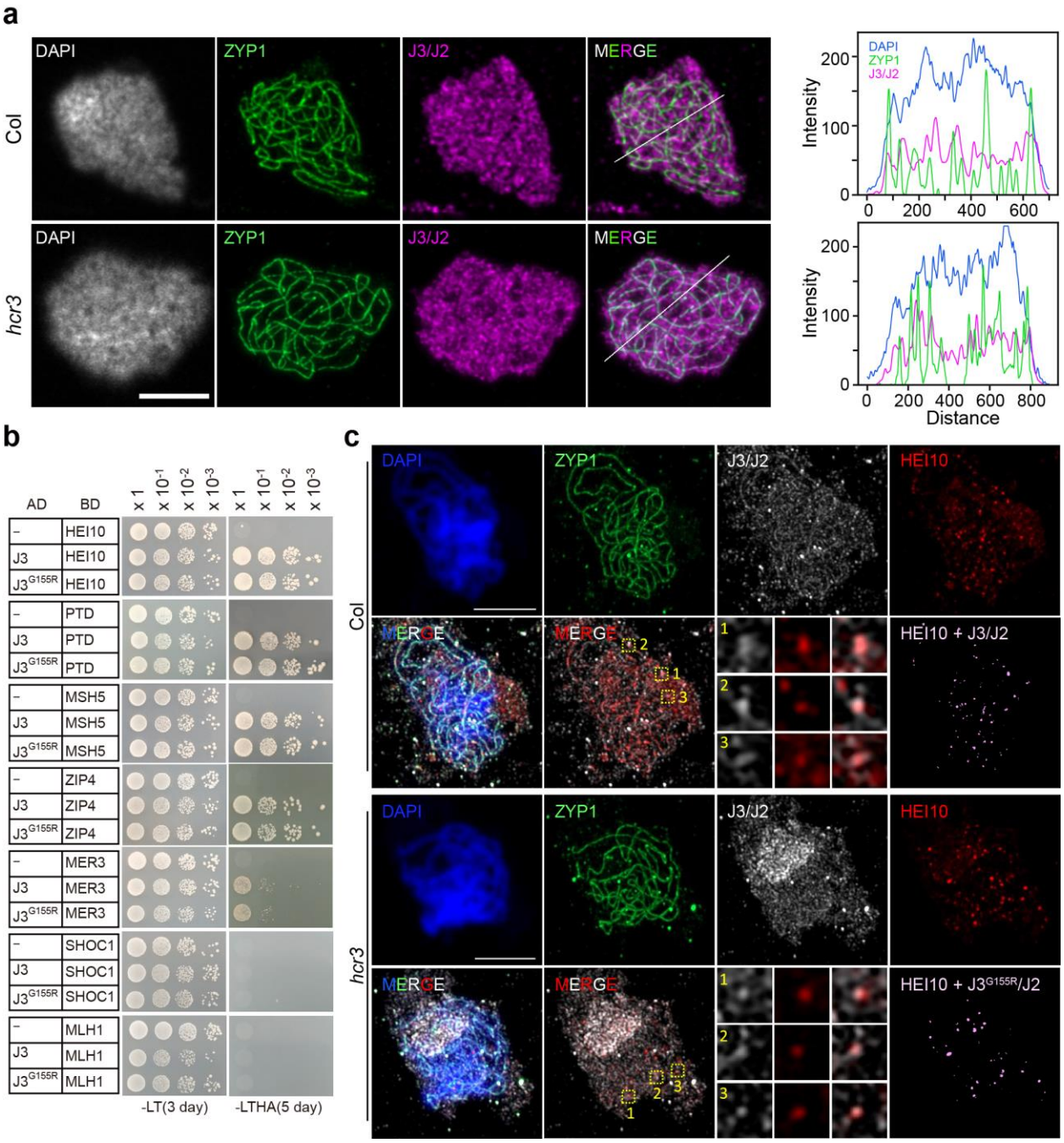

Fig. 6. J3 interacts with ZMMs and co-localizes with HEI10. a, Representative images and signal intensity plots of co-immunostained J3/J2 (magenta) and ZYP1 (green) at the pachytene stage in wild-type Col and *hcr3*. Nuclear DNA was stained with DAPI (white in images, blue in plots). Representative bisecting white lines in merged images show plot profiles of intensities and positions for DAPI (blue), ZYP1 (green), and J3/J2 (magenta). Scale bar = 5μm. **b,** Yeast two-hybrid assay showing the interaction of J3 and $J3^{G155R}$ with ZMM proteins. **c,** Representative images of co-immunostained J3/J2 (white), ZYP1 (green), and HEI10 (red) at mid-pachytene stage in wild-type Col and *hcr3*. Three yellow dot boxes (1, 2, 3) in merged images of co-immunostained J3/J2 and HEI10 are enlarged and shown. Scale bar = 5μm.

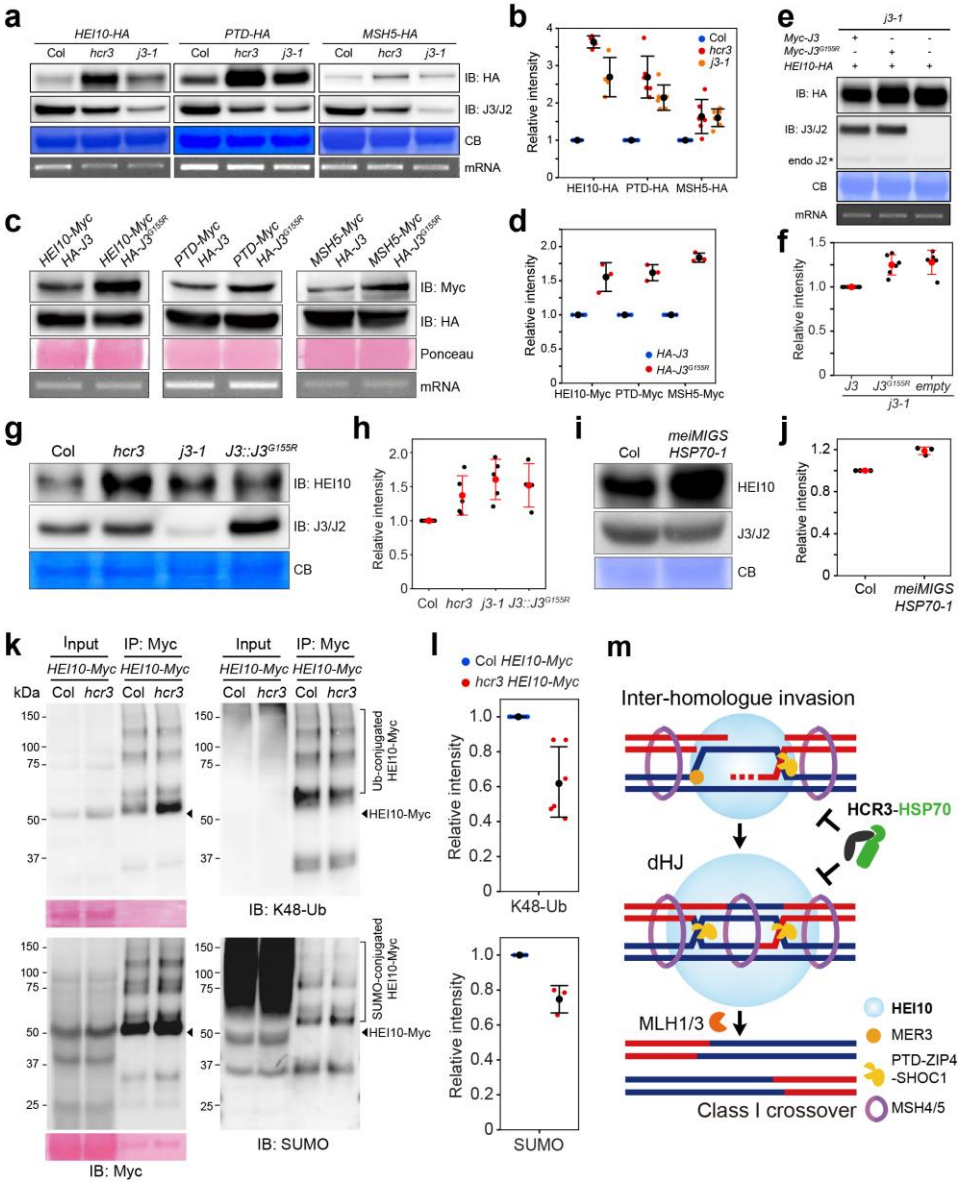

Fig. 7. HCR3 mediates proteolysis of HEI10. a and **b,** Immunoblot (**a**) and quantification **(b**) analyses of epitope-tagged HEI10, PTD, MSH5, and J3 in Col, *hcr3*, and *j3-1* protoplasts. **c** and **d,** Immunoblot (**c**) and quantification (**d**) analyses of epitope-tagged HEI10, PTD, and MSH5 in flower buds of plants co-expressing *HA-J3* or *HA-J3*^{G155R}. **e** and **f,** As for (**a** and **b**) but showing epitope-tagged HEI10, J3, and J3^{G155R} in *j3-1* protoplasts. Transcript levels of mRNA (**a, c, e**) were shown and used to calculate relative protein intensities (**b, d, f**). **g** and **h,** Immunoblot (**g**) and quantification (**h**) analyses of HEI10 in Col, *hcr3*, *j3-1*, *J3::J3*^{G155R}. **i** and **j,** As for (**g**) and (**h**) but showing in Col and *meiMIGS-HSP70-1* plants. **k** and **l,** Co-immunoprecipitation and followed by immunoblot (**k**) and quantification (**l**) analyses of ubiquitin- and SUMO-conjugated HEI10-Myc in *HEI10::HEI10-Myc* and *hcr3 HEI10::HEI10-Myc* plants. IP, immunoprecipitation, IB, immunoblot. Black (**b, d, i**) or red (**f, h, j**) dots and horizontal lines indicate mean ± s.d. of normalized intensities of immunoblot replicates (one-sided Welch's test). Colored (**b, d, i**) or black (**f, h, j**) dots represent the normalized intensities of immunoblot replicates ($n \geq 3$). **m,** A model for the role of the HCR3-HSP70 chaperone network in limiting crossovers by promoting HEI10 degradation.

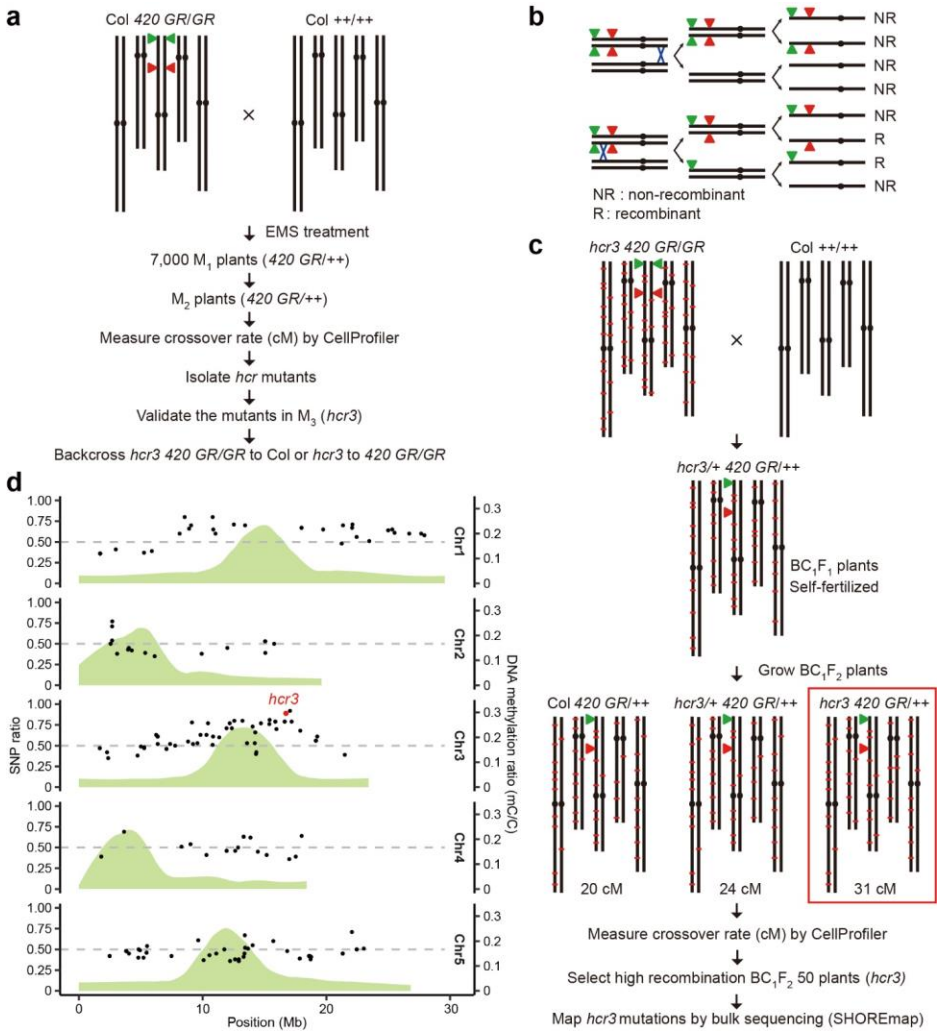

Extended Data Fig. 1. Genetic isolation and mapping of *hcr3*. a, Schematic of the genetic screen of *hcr3* mutant using *420* seed fluorescence reporter and ethylmethane sulfonate (EMS)-mediated mutagenesis. **b,** Segregation of fluorescent genes during meiosis in *420 GR/++* reporter line. **c,** Schematic of the generation of the *hcr3 420* BC_1F_2 mapping population. Red lines indicate EMS-driven mutations. **d,** Analysis of EMS allele frequency of *hcr3* BC_1F_2 segregants using SHOREmap pipeline. Black dots indicate the EMS-driven mutation sites and the red dot indicates the location of *hcr3* mutation.

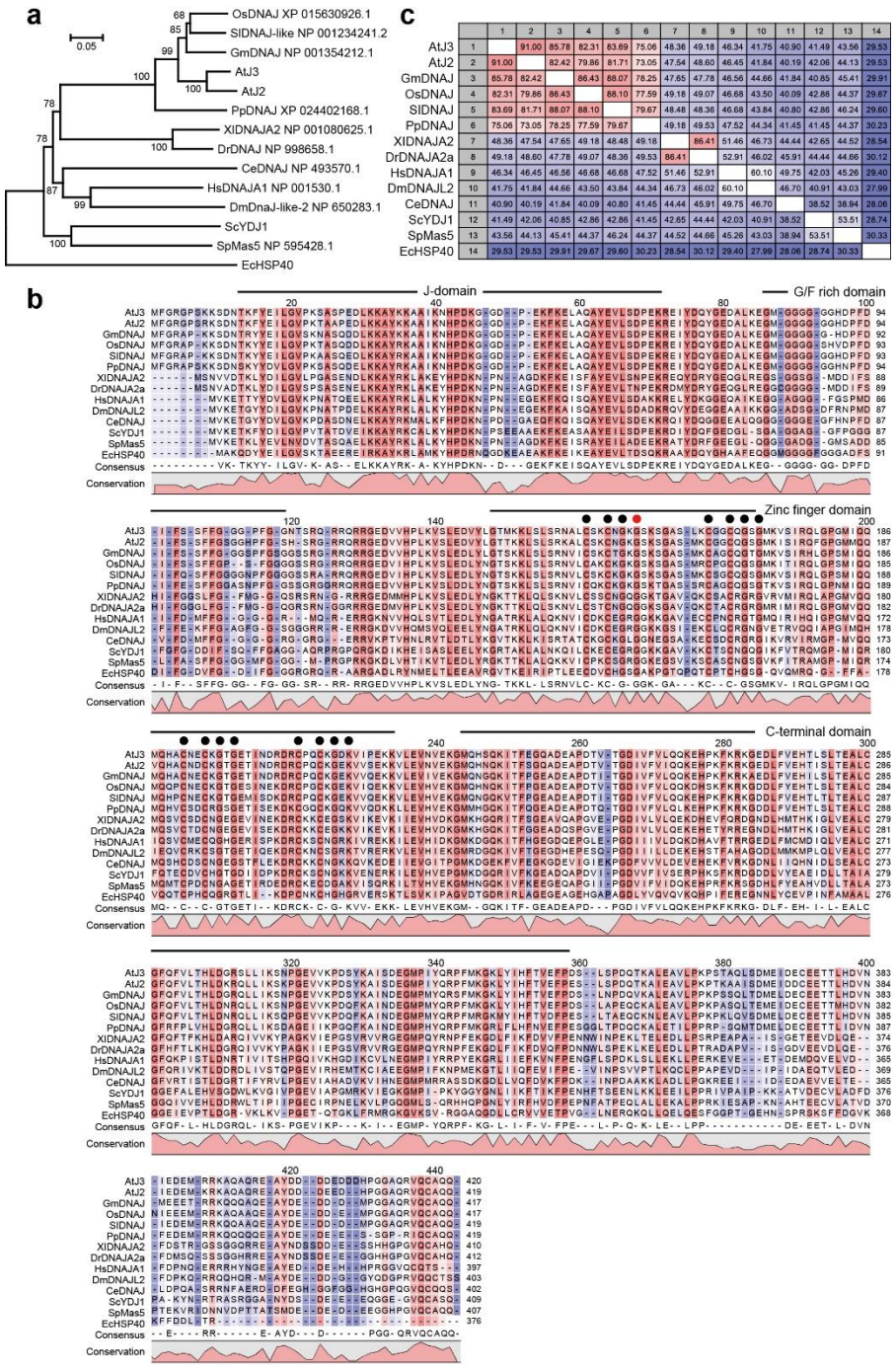

Extended Data Fig. 2. J3 proteins from diverse organisms. a, Phylogenetic tree of J3 proteins based on an alignment of amino acids. The scale bar indicates the number of changes per amino acid positions. **b,** Amino acid sequence alignment of *Arabidopsis* J3 and its homologs from diverse eukaryotic species. The conserved regions of J-domain, G/F rich domain, zinc finger domain and C-terminal domain were marked by the upper lines. Black dots indicate the conserved amino acids residing in zinc finger domain. The red dot represents the *hcr3* mutation site. **c,** As for (**b**) but showing the percentage identity of amino acid sequence between J3 homologs.

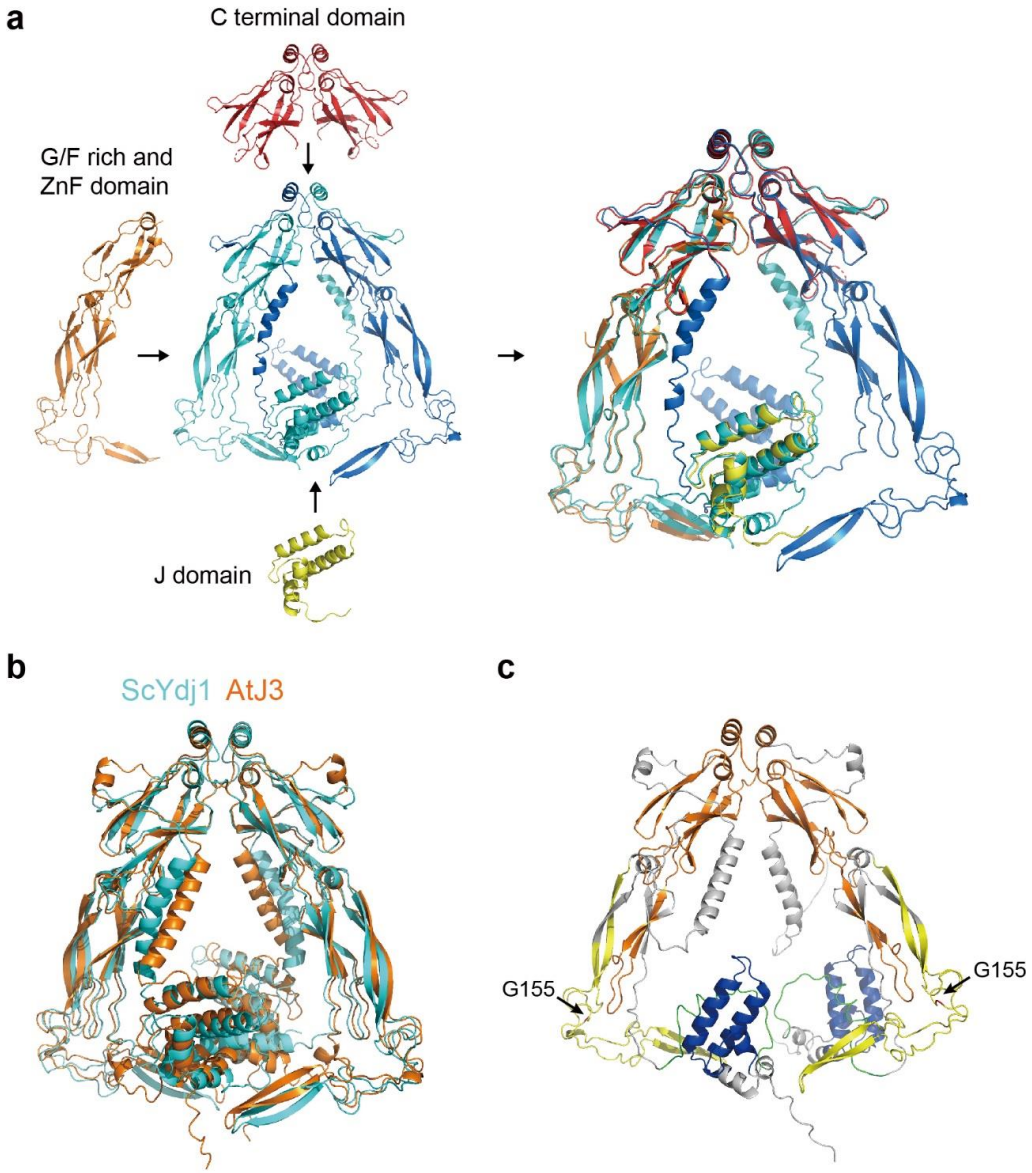

Extended Data Fig. 3. Predicted protein structures of class A HSP40 in yeast and Arabidopsis. a, AlphaFold2-simulated yeast Ydj1 (cyan, blue) and crystal structures for J-domain (yellow), G/F rich-ZnF (brown) and client binding domain and C-terminal dimerization domain (red). **b,** Overlay of AlphaFold2-simulated yeast Ydj1 (cyan) and Arabidopsis J3 (brown) protein structures. **c,** AlphaFold2-simulated Arabidopsis J3 dimer. The substitution positions (glycine, G155) of J3 in *hcr3* are indicated by arrows.

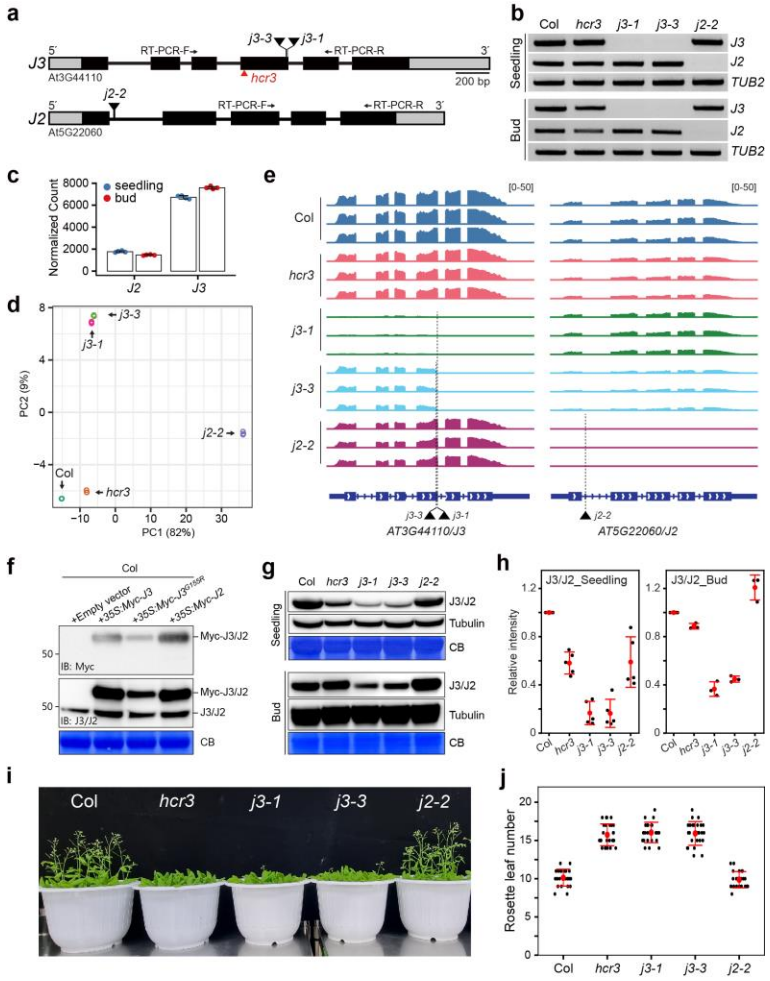

Extended Data Fig. 4. Characterization of *j3* and *j2* T-DNA insertion mutants. a, Gene structures for *J3* and *J2*. Positions of T-DNA insertion (black triangles), *hcr3* mutation (red triangle), and RT-PCR primers (arrows) are shown. **b,** Agarose gels showing RT-PCR products of *J3* and *J2* in Col, *hcr3*, *j3-1*, *j3-3*, and *j2-2*. **c,** Plot showing normalized transcript reads for *J3* and *J2* in RNA-seq of Col seedlings and buds. **d,** Principle component analysis of three replicates of RNA-seq libraries in Col, *hcr3*, *j3-1*, *j3-3*, and *j2-2* seedlings. **e,** As for (**d**) but showing integrative genomic viewer windows showing the transcript levels for *J3* and *J2*. **f,** Immunoblot analysis of transiently expressed epitope Myc-tagged and endogenous J3 and J2 in Col protoplasts. IB, immunoblot. CB, Coomassie blue. Anti-J3 antibody detects both J3 and J2 proteins (J3/J2). **g** and **h,** Immunoblot (**g**) and quantification (**h**) analyses of J3/J2 using anti-J3 antibody in seedlings and buds of Col, *hcr3*, *j3-1*, *j3-3*, and *j2-2*. Immunoblots of tubulin and Coomassie blue staining were used for loading control and quantification. Red dots and horizontal lines indicate mean ± s.d. of intensities of immunoblot replicates (one-sided Welch's *t*-test). Black dots represent the normalized intensities of immunoblot replicates ($n \geq 3$). **i** and **j,** Representative images (**i**) and quantification (**j**) of flowering time in Col, *hcr3*, *j3-1*, *j3-3*, and *j2-2*. Plants were grown under long-day conditions, and rosette leaf number was counted to measure flowering time. Red dots and horizontal lines indicate mean ± s.d. of leaf number from individual plants (one-sided Welch's *t*-test). Black dots represent leaf number of individual plants.

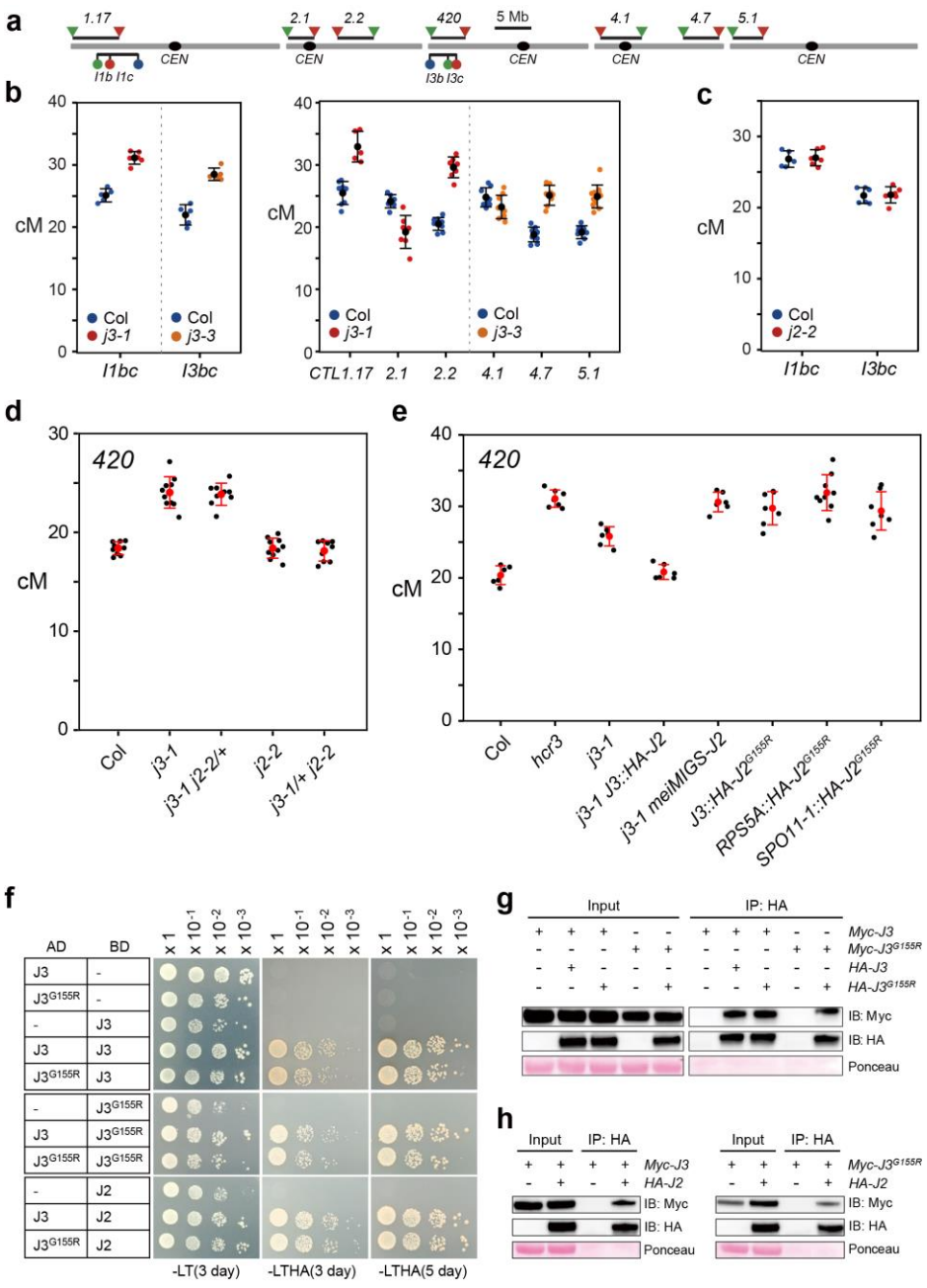

Extended Data Fig. 5. Functional redundancy between *J3* and *J2* in meiotic crossover frequency. a, Seed (triangles) and pollen (circles) FTLs across the *Arabidopsis* genome. Lines represent the interval positions. **b** and **c,** Crossover frequency (cM) of pollen (**b**) and seed (**c**) FTLs in Col, *j3-1*, *j3-3* and *j2-2*. **d,** *420* crossover frequency (cM) in Col, *j3-1*, *j3-1*, *j2-2/+ j2-2*, and *j3-1/+ j2-2*. **e,** As for (**d**) but showing Col, *hcr3*, *j3-1*, *j3-1 J3::HA-J2* (T_1), *j3-1 meiMIGS-J2* (T_1), and transgenic plants (T_1) expressing *HA-J2*^{G156R} under the *J3*, *RPS5A*, and *SPO11-1* promoters. Black (**b, c**) or red (**d, e**) dots and horizontal lines indicate mean ± s.d. of cM values from individual plants (one-sided Welch's *t*-test). Colored (**b, c**) or black (**d, e**) dots represent cM values of individual plants. **f,** Yeast two-hybrid analysis showing protein interactions of J3 and J3^{G155R} with themselves and J2. **g** and **h,** Co-immunoprecipitation analysis showing dimerization of J3 and J3^{G155R} with themselves (**g**) and J2 (**h**) in *Arabidopsis* protoplasts.

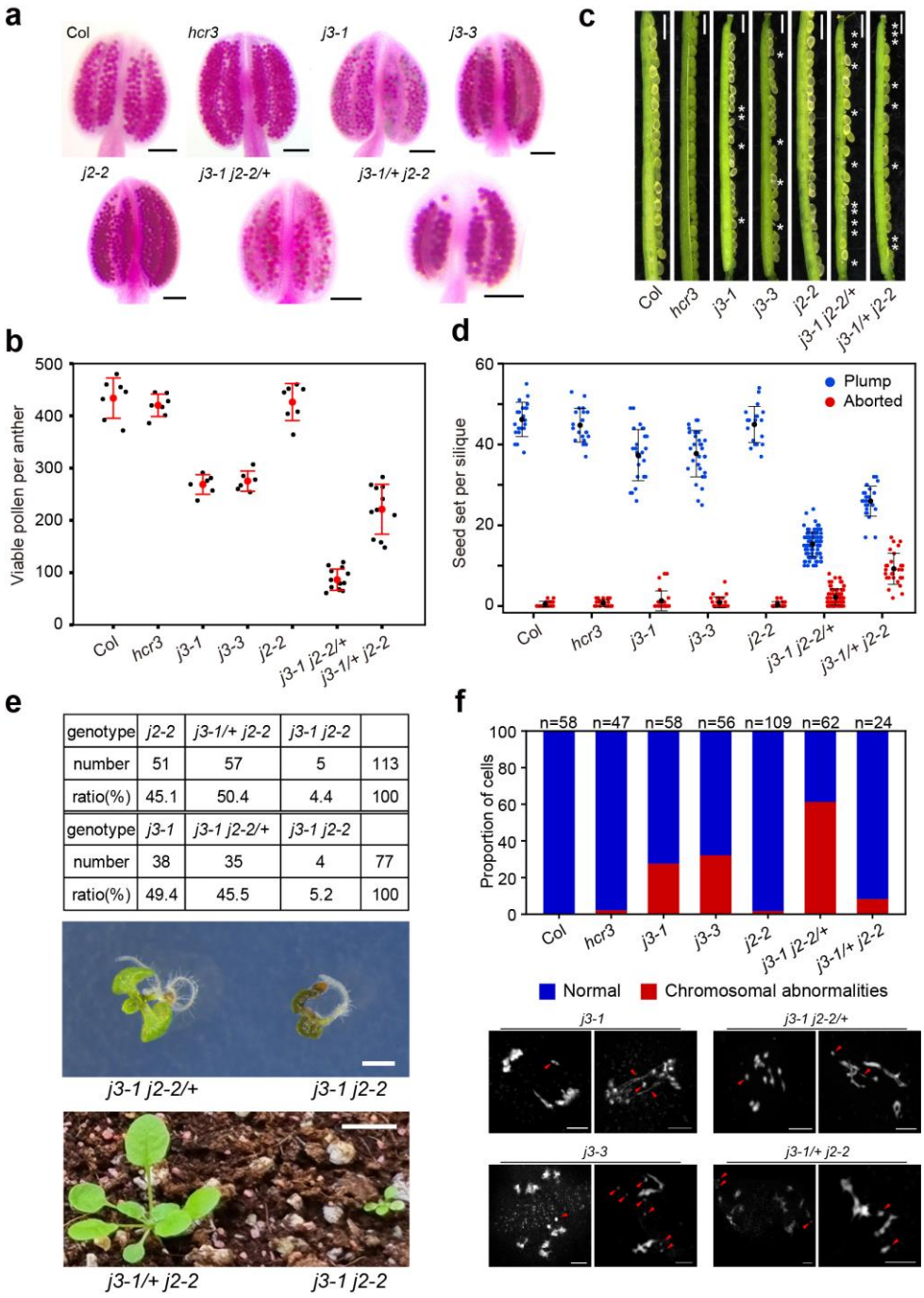

Extended Data Fig. 6. Functional redundancy between *J3* and *J2* in pollen development, embryogenesis, and meiotic chromosome segregation. a and **b,** Anthers containing Alexander-stained pollen grains (**a**) and plot (**b**) showing viable pollen grains per anther in Col, *hcr3*, *j3-1*, *j3-3*, *j2-2*, *j3-1 j2-2/+*, and *j3-1/+ j2-2*. Scale bars, 100 μm. **c** and **d,** As for (**a** and **b**) but showing representative images (**c**) and plot (**d**) for number of seeds per silique. White asterisks indicate aborted seeds. Scale bars, 1 mm. **e,** Table of genotyping results and representative images showing seedling lethality of *j3-1 j2-2* from the progeny of self-fertilized *j3-1 j2-2/+* and *j3-1/+ j2-2*. Scale bars, 1 mm (top), 1 cm (bottom). **f,** As for (**e**) but showing plot and representative DAPI-stained images of chromosomal abnormalities at metaphase I or anaphase I. Red arrows indicate chromosome fragmentation or interlock. Scale bars, 5 μm.

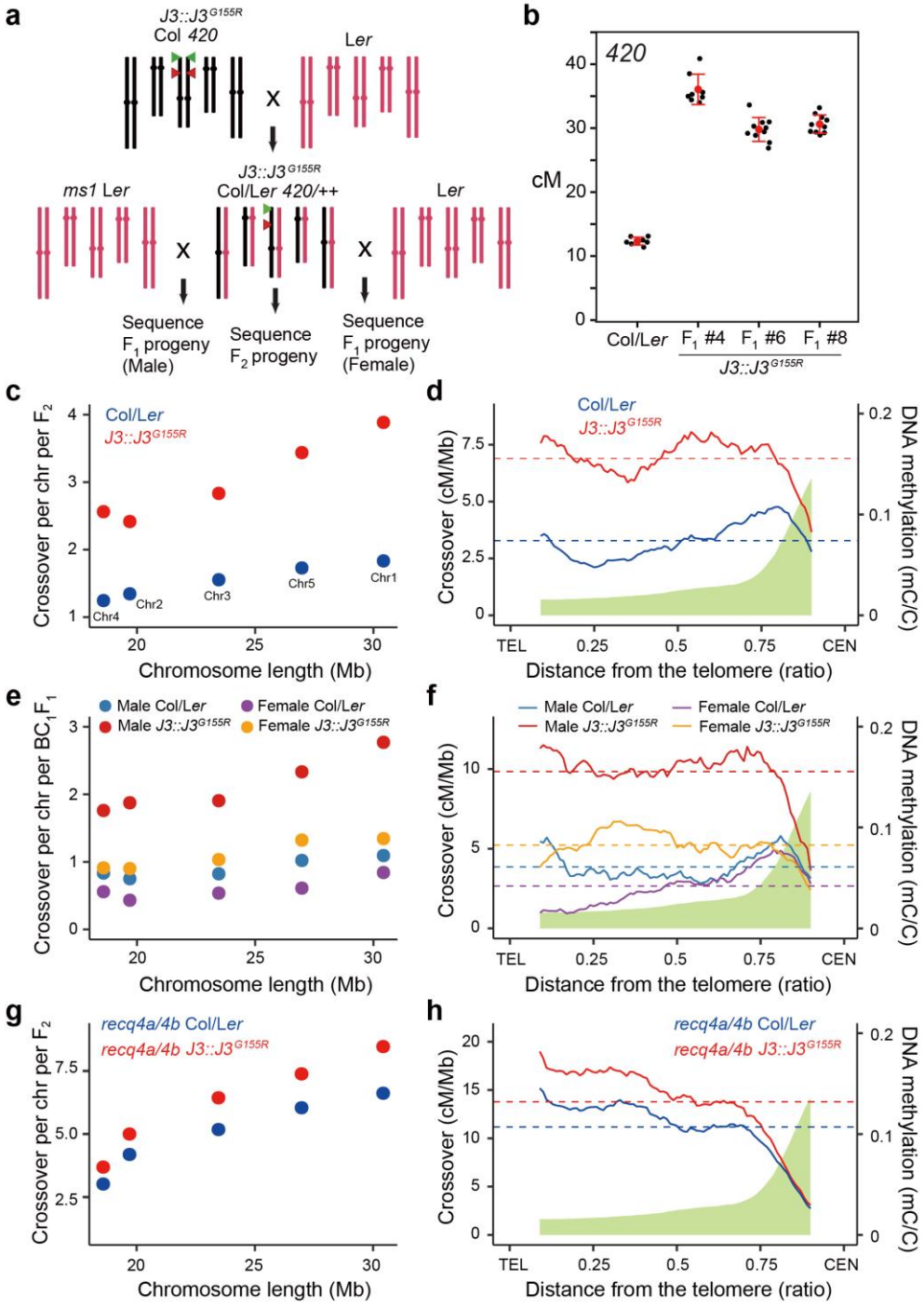

Extended Data Fig. 7. Genomic analyses for crossover number and distribution in Col×L*er* and *J3::J3*^{G155R} Col×L*er*. a, Schematic of generation of *J3::J3*^{G155R} Col×L*er* hybrid plants and crossover map populations. **b,** *420* crossover frequencies in Col×L*er* and *J3::J3*^{G155R} Col×L*er* F_1 hybrid plants. **c,** Average crossover number per chromosome in Col×Ler and *J3::J3*^{G155R} Col×L*er* F_2 individuals. **d,** As for (**c**) but showing normalized crossover frequencies (cM/Mb) along chromosome arms from the telomere (TEL) to the centromere (CEN). **e** and **f,** As for (**c** and **d**), but showing male and female meiosis. **g** and **h,** As for (**c** and **d**), but showing *recq4a recq4b* background.

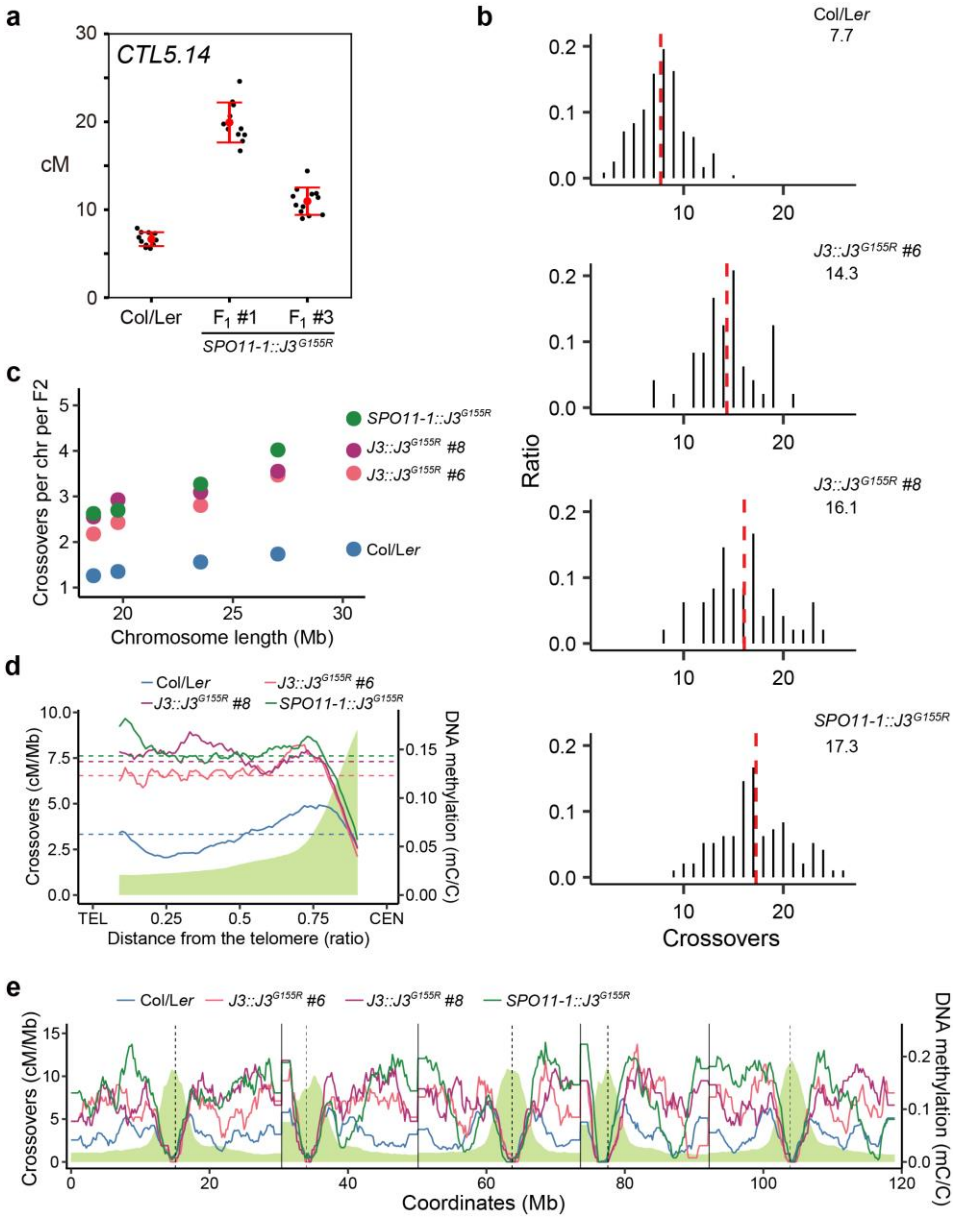

Extended Data Fig. 8. GBS of genomic maps for F_2 individuals from independent *J3::J3^{G155R}* and *SPO11-1::J3^{G155R}* Col×L*er* plants. a, *CTL5.14* crossover frequencies in Col×L*er* and two independent *SPO11-1::J3^{G155R}* Col×L*er* F_1 hybrid plants. **b,** Histograms showing the ratio of F_2 individuals containing different crossover numbers in each population. Vertical dotted red lines indicate the mean value. **c,** Average number of crossovers per chromosome in F_2 individuals in each population. **d** and **e,** As for (**c**) but showing normalized crossover frequencies (cM/Mb) along chromosome arms from the telomere (TEL) to the centromere (CEN) (**d**) and across the genome (**e**).

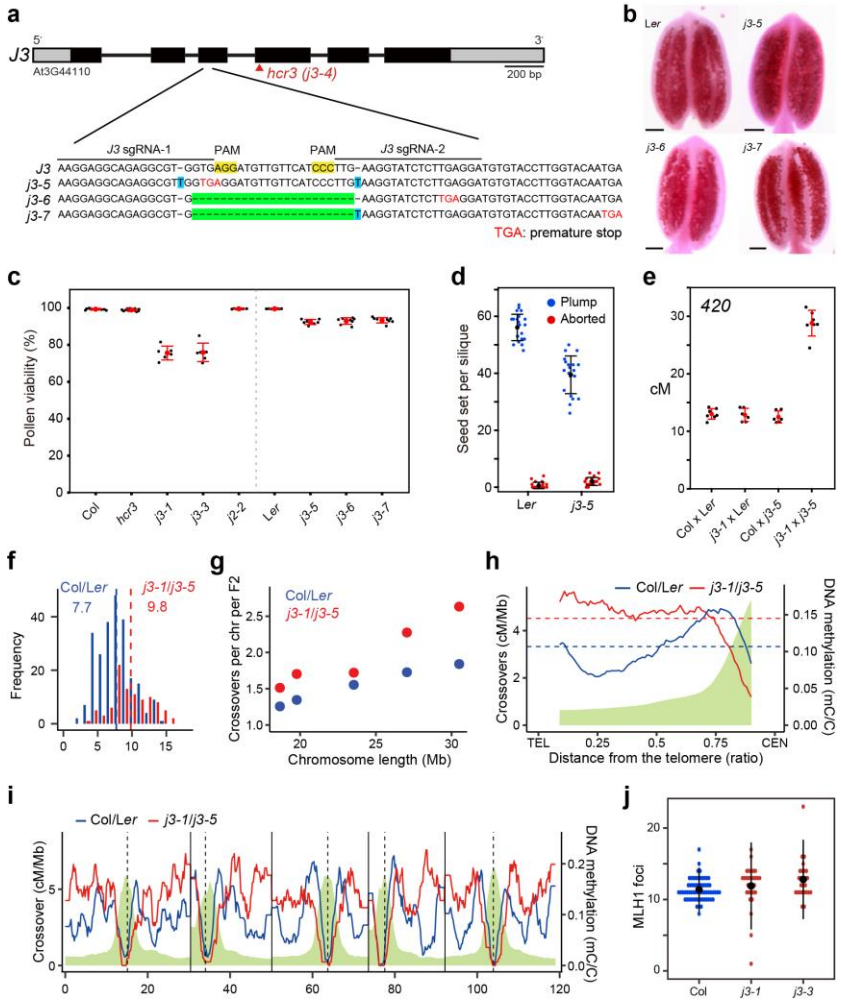

Extended Data Fig. 9. Genome-wide crossover mapping of *j3* knockout Col×L*er* hybrids and quantification of MLH1 foci in *j3* mutants. a, Gene structure and nucleotide sequences of *J3* with *hcr3* mutation (red triangle), positions of CRISPR/Cas9 sgRNAs, and Cas9-mediated mutations for the three *j3* null mutants in L*er*. Nucleotide deletions and insertions are highlighted in green and blue, respectively. **b,** Anthers containing Alexander-stained pollen grains of L*er*, *j3-5*, *j3-6*, and *j3-7*. Scale bars, 100 μm. **c,** As for (**b**) but showing plot of pollen viability in Col, *hcr3*, *j3-1*, *j3-3*, *j2-2*, L*er*, *j3-5*, *j3-6*, and *j3-7*. **d,** Number of seeds per silique in L*er* and *j3-5*.**e,** *420* crossover frequency (cM) in Col×L*er* (Col/L*er*), *j3-1*×L*er*, Col×*j3-5*, and *j3-1*×*j3-5* F_1 hybrids. **f,** Histogram of sex-averaged crossover number in Col/L*er* (blue, n = 240) and *j3-1*/*j3-5* (red, n = 96) F_2 individuals. **g,** As for (**f**) but showing average crossover number per chromosome. **h** and **i,** As for (**f**) but showing normalized crossover frequencies (cM/Mb) along chromosome arms from the telomere (TEL) to the centromere (CEN) (**h**) and across the genome (**i**). **j,** Plot showing quantification of immunostained MLH1 foci of pollen mother cells at diplotene stage in Col, *j3-1*, and *j3-3*. Black dots and horizontal lines indicate mean ± s.d. of values (Wilcoxon test, *j3-1* P=1.15×10^{-2}, *j3-3* P=5.88×10^{-3}).

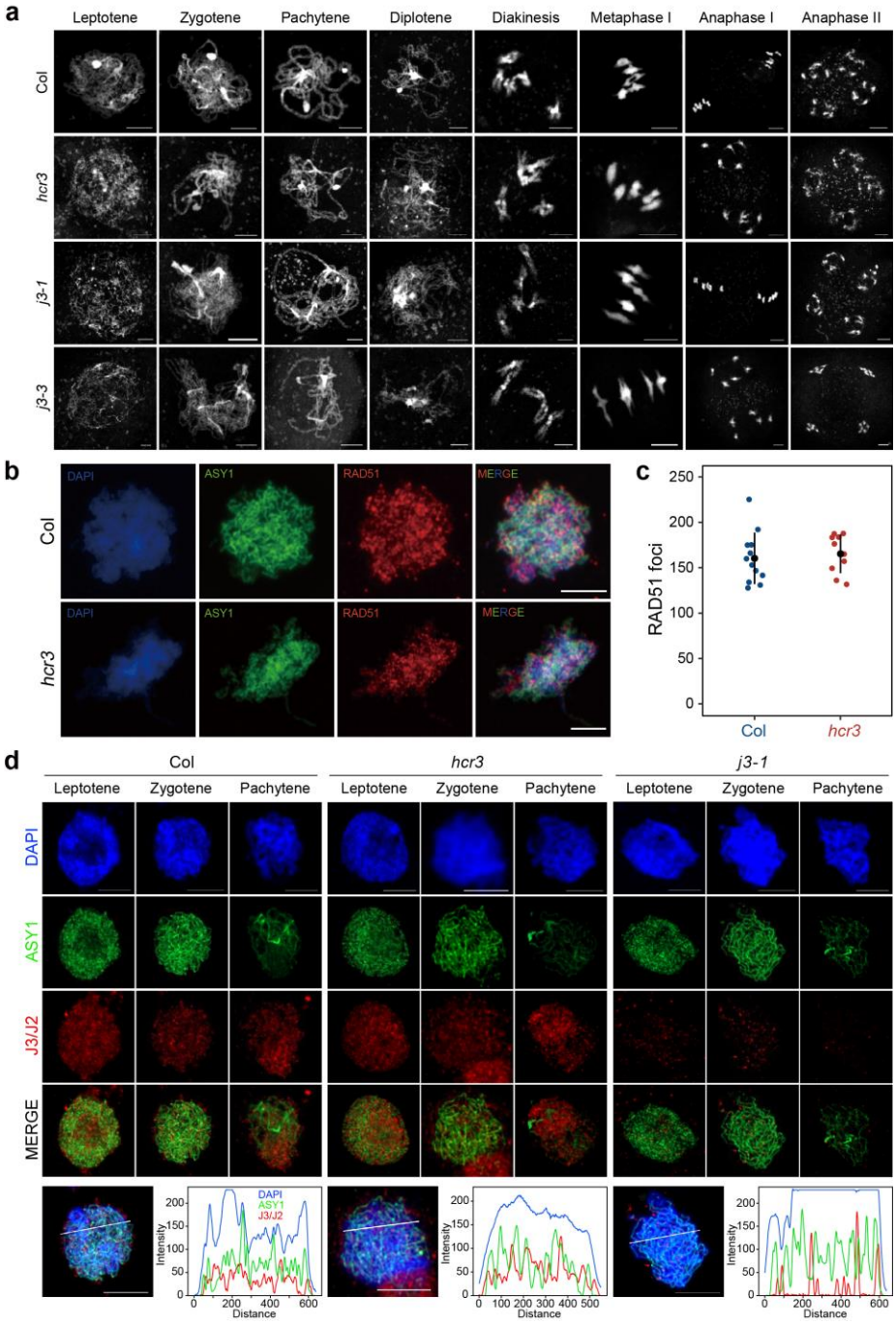

Extended Data Fig. 10. Chromosome behavior and immunostaining of ASY1, RAD51, and J3 foci in wild type, *hcr3*, and *j3*. a, Representative images of male meiocytes spread and stained with DAPI in Col, *hcr3*, *j3-1*, and *j3-3*. **b,** Representative images of ASY1 (green) and RAD51 (red) immunostaining in Col and *hcr3* male meiocytes. Nuclei spreads were stained with DAPI. Scale bars, 10 μm. **c,** Quantification of RAD51 foci number per cell in Col and *hcr3*. **d,** Immunostaining of ASY1 (green) and J3/J2 (red) during meiotic prophase I in Col, *hcr3* and *j3-1*. Representative bisecting lines in merged zygotene images show plot profiles of intensities and positions for DAPI (blue), ASY1(green), and J3/J2 (red). Nuclear DNA was stained with DAPI (blue). Scale bars, 5 μm.

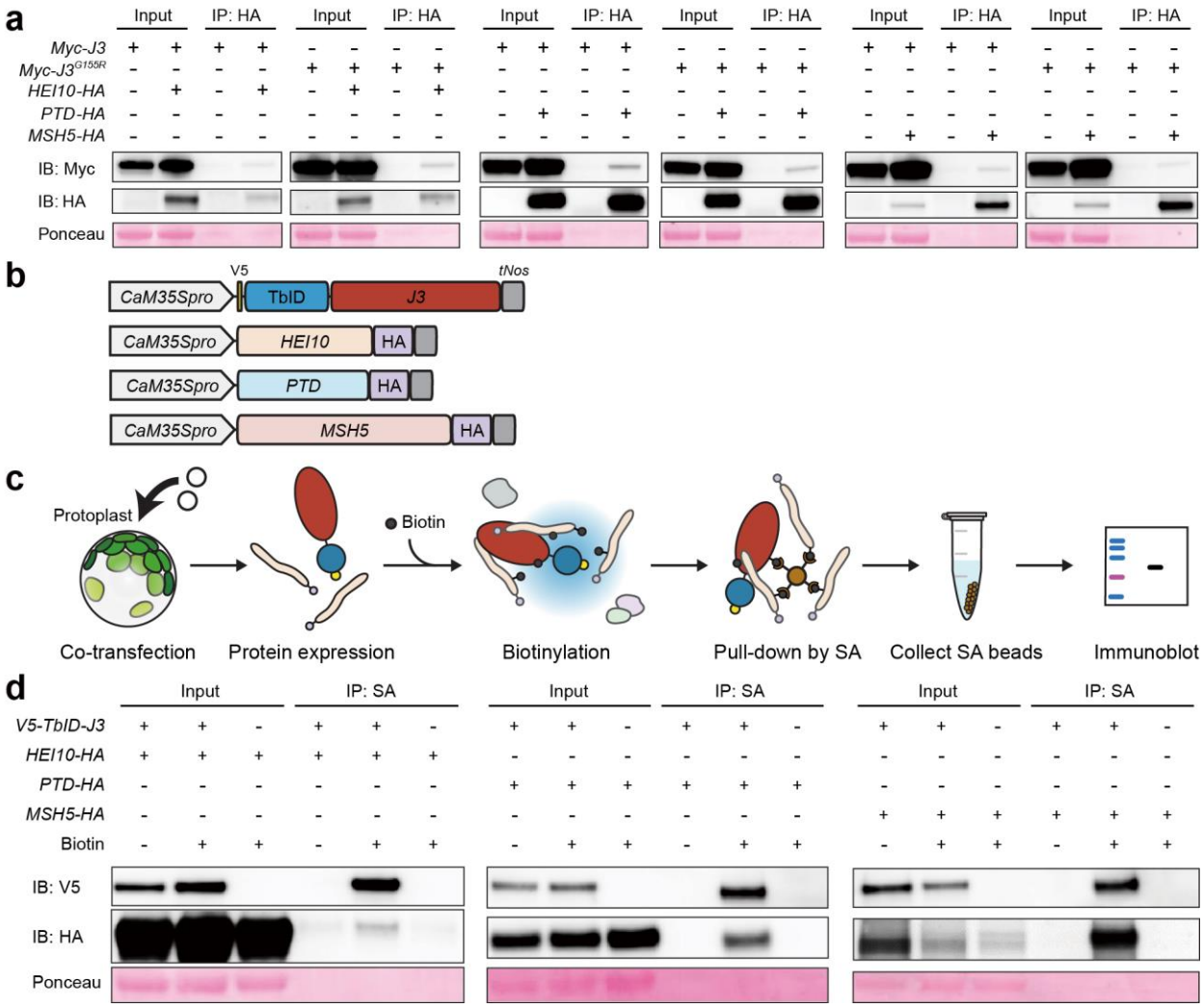

Extended Data Fig. 11. TurboID-J3-mediated proximity labeling of HEI10, PTD and MSH5 proteins in *Arabidopsis* protoplasts. a, Co-immunoprecipitation of J3 and J3^{G155R} with HEI10, PTD and MSH5 in protoplasts. **b,** Plasmid constructs of *Arabidopsis* protoplast transient expression for TurboID-based proximity labeling. **c,** Diagram of proximity labeling in *Arabidopsis* protoplasts. **d,** Immunoprecipitation and immunoblot analysis of HEI10, PTD and MSH5 in protoplasts co-expressing TurboID-J3 without (-) and with (+) biotin treatment. IP, immunoprecipitation; SA, streptavidin. Ponceau S-stained membrane was shown as a loading control.

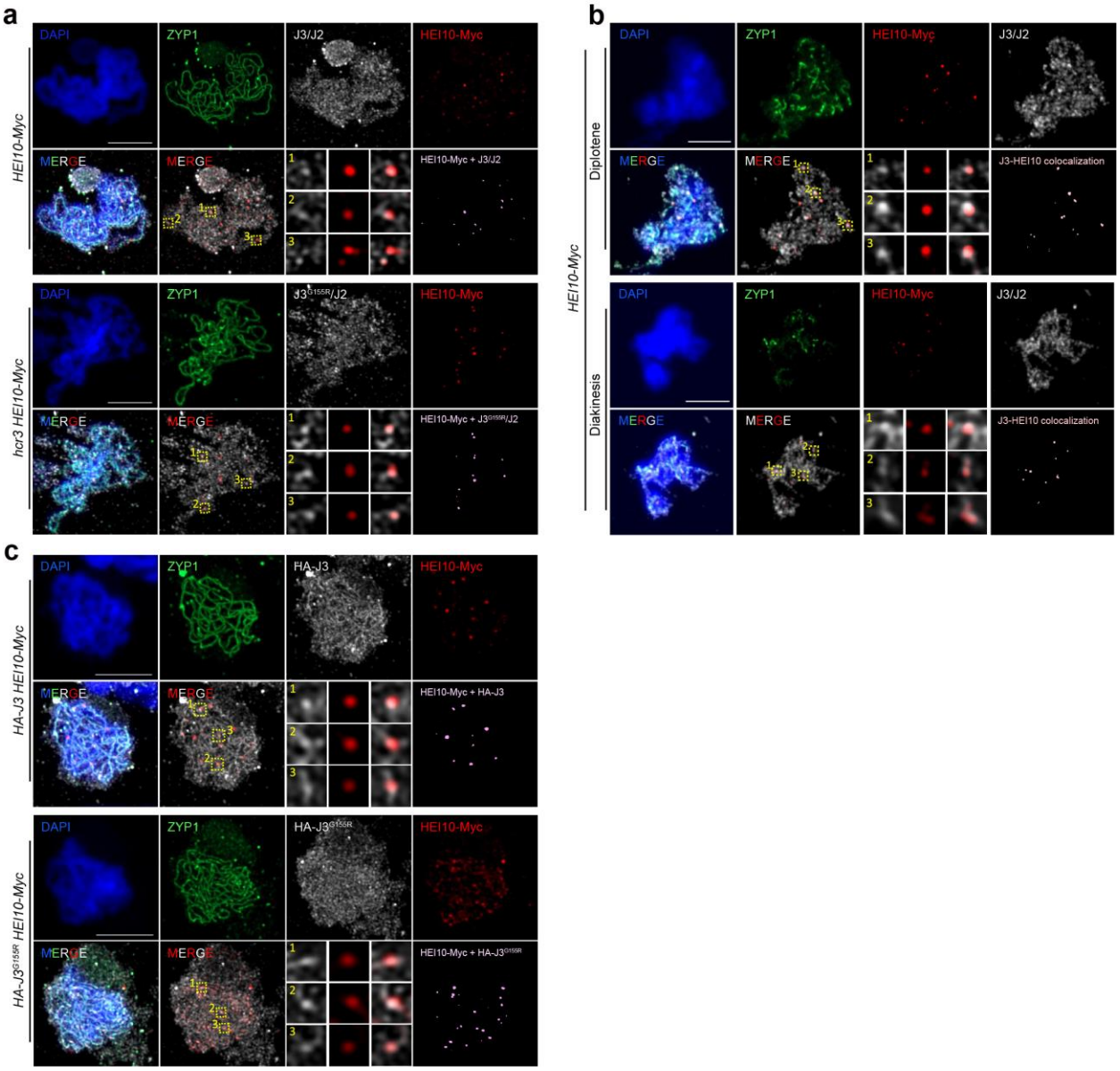

Extended Data Fig. 12. J3 and J3^{G155R} co-localize with HEI10 *in vivo*. a, Representative images of co-immunostained J3/J2 (white), ZYP1 (green), and HEI10-Myc (red) at late-pachytene stage in Col *HEI10::HEI10-Myc* and *hcr3 HEI10::HEI10-Myc*. **b,** As for (**a**) but showing at diplotene and diakinesis stage in Col *HEI10::HEI10-Myc*. **c,** As for (**a**) but showing immunostained HA-J3, HA-J3^{G155R}, and HEI10-Myc at late-pachytene stage in *J3::HA-J3 HEI10::HEI10-Myc* and at mid-pachytene stage in *J3::HA-J3^{G155R} HEI10::HEI10-Myc* plants. Three yellow dotted line boxes (1, 2, 3) in the merged images of co-immunostained J3/J2 and HEI10 are enlarged and displayed. Scale bars, 5 μm.

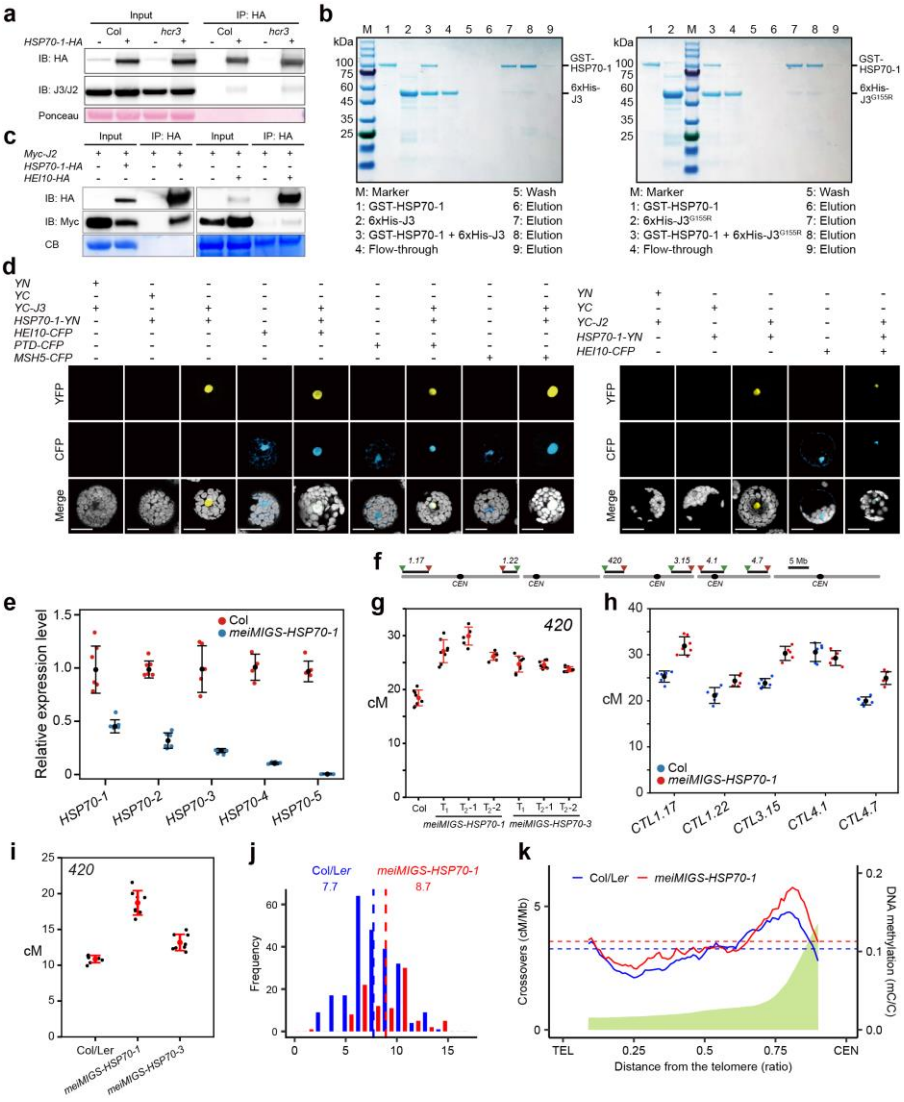

Extended Data Fig. 13. J3-HSP70 chaperone machinery restricts crossover frequency. a, Co-immunoprecipitation analysis of J3 and HSP70 in *Arabidopsis* protoplasts. **b,** *In vitro* pull-down assay of J3 and HSP70-1. **c,** Co-immunoprecipitation analysis of J2 with HSP70 and HEI10 in *Arabidopsis* protoplasts. **d,** Co-localization of J3/J2 and HSP70 with HEI10, PTD, and MSH5 in *Arabidopsis* protoplasts. YN indicates N-terminal 1-158 amino acid resides of yellow fluorescent protein (YFP) and YC, C-terminal 159-238 amino acid residues of YFP for BiFC assay. Scale bars, 20 μm.**e,** RT-qPCR analysis of *HSP70-1-5* genes in unopen flower buds of Col and *meiMIGS-HSP70-1* plants. Red and blue dots indicate biological replicates (n = 6). Mean ± s.d. of values are shown by black dots and horizontal lines. **f,** Seed FTLs across genome. **g,** *420* crossover frequencies in *meiMIGS-HSP70-1* and *meiMIGS-HSP70-3* transgenic lines. **h,** As for (**g**) but showing FTLs in *meiMIGS-HSP70-1*. **i,** As for (**g**) but showing *meiMIGS-HSP70*/L*er* hybrid plants. **j,** Histogram of crossover number in Col×L*er* (blue, n = 240) and *meiMIGS-HSP70-1*×L*er* (red, n = 96) F_2 individuals. Dotted blue and red lines indicate mean values. **k,** As for (**j**) but showing normalized crossover frequencies (cM/Mb) along chromosome arms from the telomere (TEL) to the centromere (CEN). Black (**g, i**) or colored (**h**) dots indicate cM values of individual plants. Red (**g, i**) or black (**h**) dots and horizontal lines represent mean ± s.d. of cM values from individual plants (one-sided Welch's t-test). n ≥ 6 plants of biological replicates.

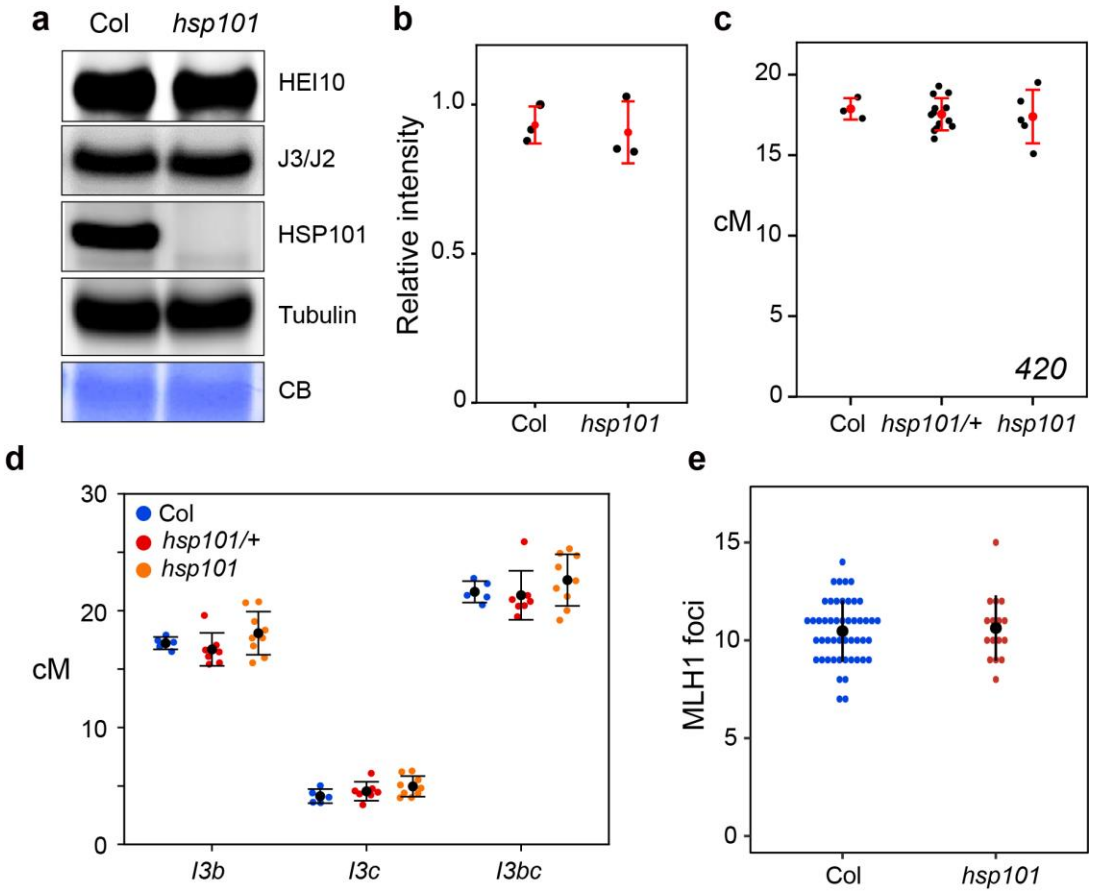

Extended Data Fig. 14. Normal HEI10 abundance, crossover frequencies of FTLs, and MLH1 foci in *hsp101* mutants. a and **b,** Immunoblot (**a**) and quantification (**b**) analysis of HEI10 in *hsp101*. Red dots and horizontal lines indicate mean ± s.d. of normalized intensities of immunoblot replicates (one-sided Welch's *t*-test). Black dots indicate normalized intensities of immunoblot replicates ($n = 3$). (**b**, *t*-test, $P = 0.74$). **c** and **d,** Crossover frequencies of seed (**c**) and pollen (**d**) FTLs in *hsp101*. Black (**c**) or colored (**d**) dots indicate cM values of individual plants. Red (**c**) or black (**d**) dots and horizontal lines represent mean ± s.d. of cM values from individual plants (one-sided Welch's *t*-test). $n \geq 3$ plants of biological replicates. (**c**,**d**, *t*-test, all $P > 0.6$) **e,** Quantification of immunostained MLH1 foci per cell at diplotene stage in Col and *hsp101*. Black dots and horizontal lines indicate mean ± s.d. of values (Wilcoxon test, $P = 0.92$).

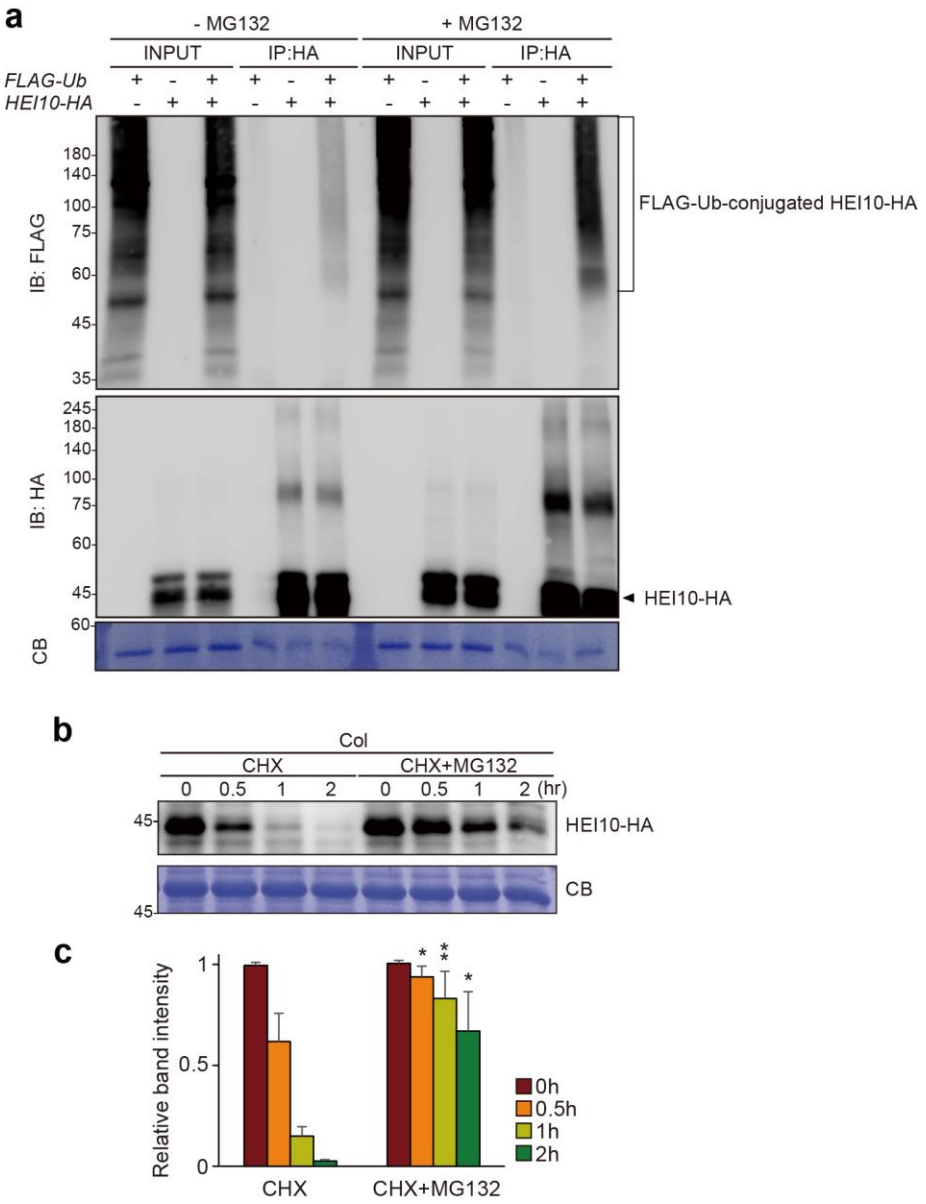

Extended Data Fig. 15. Ubiquitination modification and proteasome-dependent degradation of HEI10 in *Arabidopsis* protoplasts. a, Immunoprecipitation and immunoblot analysis of ubiquitin (Ub)-conjugated HEI10-HA in *Arabidopsis* protoplasts. The plasmid constructs for either FLAG-tagged ubiquitin (FLAG-Ub) or HEI10-HA, or both were co-transfected into protoplasts. IP, immunoprecipitation. IB, immunoblot. Coomassie blue (CB) stained membrane is shown as a loading control. **b** and **c,** Immunoblot analysis (**b**) and quantification plot (**c**) of HEI10-HA protein upon treatment of translation elongation (cycloheximide, CHX) and proteasome (MG132) inhibitors in *Arabidopsis* protoplasts. *P < 0.05 and **P < 0.01 for a one-sided Welch's *t*-test.

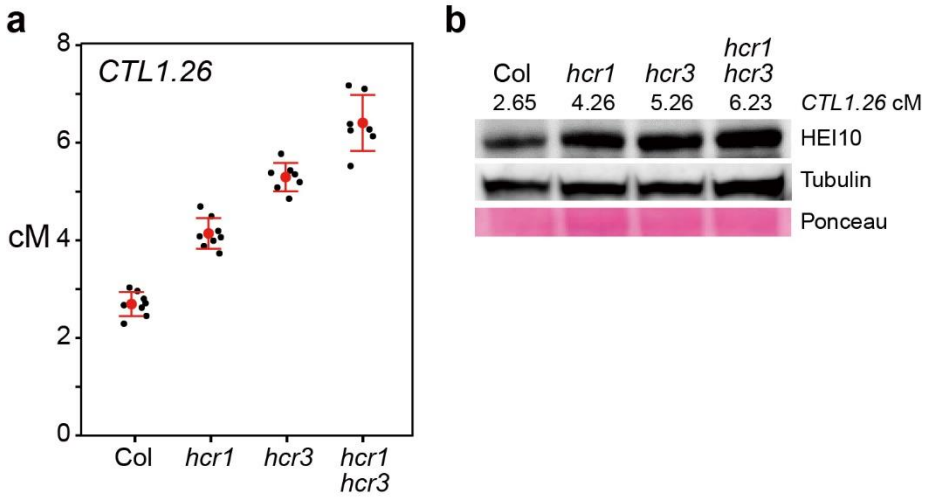

Extended Data Fig. 16. HCR1 and HCR3 are required for restricting class I crossovers. a, Crossover frequencies of *CTL1.26* in Col, *hcr1, hcr3* and *hcr1 hcr3* (Supplementary Table 27). Black dots indicate cM values of individual plants. Red dots and horizontal lines represent mean ± s.d. of cM values from individual plants (one-sided Welch's t-test). $n \geq 7$ plants of biological replicates. **b,** Immunoblot analysis of HEI10 in Col, *hcr1, hcr3* and *hcr1 hcr3*. Ponceau S-stained membrane and tubulin protein blot were shown as a loading control.